EDGEWOOD CHEMICAL BIOLOGICAL CENTER
U.S. ARMY RESEARCH, DEVELOPMENT AND ENGINEERING COMMAND
Aberdeen Proving Ground, MD 21010-5424

ECBC-TR-1385

HIGHLY RESOLVED SUB-TERAHERTZ VIBRATIONAL SPECTROSCOPY OF BIOLOGICAL MACROMOLECULES AND BACTERIA CELLS

Waleed Maswadeh
Richard Vanderbeek
Raphael Moon

RESEARCH AND TECHNOLOGY DIRECTORATE

Ashish Tripathi

LEIDOS, INC.
Gunpowder, MD 21010-0068

Aaron M. Moyer
Tatiana Globus
Boris Gelmont
Igor Sizov
Jerome Ferrance

VIBRATESS, LLC
Charlottesville, VA 22901-2213

July 2016

Disclaimer

The findings in this report are not to be construed as an official Department of the Army position unless so designated by other authorizing documents.

REPORT DOCUMENTATION PAGE

Form Approved
OMB No. 0704-0188

1. REPORT DATE *(DD-MM-YYYY)*	**2. REPORT TYPE**	**3. DATES COVERED** *(From - To)*
XX-07-2016	Final	Mar 2014 – Mar 2015

4. TITLE AND SUBTITLE
Highly Resolved Sub-Terahertz Vibrational Spectroscopy of Biological Macromolecules and Bacteria Cells

5a. CONTRACT NUMBER
W911SR-14-P-0022

5b. GRANT NUMBER

5c. PROGRAM ELEMENT NUMBER

6. AUTHOR(S)
Maswadeh, Waleed; Vanderbeek, Richard; Moon, Raphael (ECBC); Tripathi, Ashish (Leidos); Moyer, Aaron M.; Globus, Tatiana; Gelmont, Boris; Sizov, Igor; and Ferrance, Jerome (Vibratess)

5d. PROJECT NUMBER

5e. TASK NUMBER

5f. WORK UNIT NUMBER

7. PERFORMING ORGANIZATION NAME(S) AND ADDRESS(ES)
Director, ECBC, ATTN: RDCB-DRI-S, APG, MD 21010-5424
Leidos, Inc.; P.O. Box 68; Gunpowder, MD 21010-0068
Vibratess, LLC; 104 Chaucer Road; Charlottesville, VA 22901-2213

8. PERFORMING ORGANIZATION REPORT NUMBER
ECBC-TR-1385

9. SPONSORING / MONITORING AGENCY NAME(S) AND ADDRESS(ES)
Defense Threat Reduction Agency; 8725 John J. Kingman Road, MSC 6201; Fort Belvoir, VA 22060-6201

10. SPONSOR/MONITOR'S ACRONYM(S)
DTRA

11. SPONSOR/MONITOR'S REPORT NUMBER(S)

12. DISTRIBUTION / AVAILABILITY STATEMENT
Approved for public release; distribution is unlimited.

13. SUPPLEMENTARY NOTES

14. ABSTRACT:
Sub-terahertz (sub-THz) vibrational spectroscopy for biodetection is based on specific resonance features and vibrational modes or groups of modes at close frequencies that are in the absorption (transmission) spectra of large biological molecules and intact bacterial cells and spores. Improvements in sensitivity, especially in the discriminative capability of sub-THz vibrational spectroscopy for detection, characterization, and identification of bacterial organisms, require higher spectral resolution to resolve the spectral features. Herein we describe a new, continuous-wave and frequency-domain spectroscopy sensor with imaging capability. This spectroscopy system was operated at room temperature in the sub-THz spectral region between 315 and 480 GHz. We present experimental spectra obtained from biological macromolecules and species using this spectrometer, and we compare biological spectra with simulation results using molecular dynamics. Observed, multiple, intense and specific resonances in transmission and absorption spectra from nanogram samples with spectral line widths as small as 0.1−1 cm provide the conditions for determining reliable discriminative capability and for monitoring interactions between biomaterials and reagents in near real time.

15. SUBJECT TERMS
Biological cells
Sub-terahertz (sub-THz) vibrational spectroscopy
Modeling
Biosensor
Molecular components
Frequency resolution

16. SECURITY CLASSIFICATION OF:			**17. LIMITATION OF ABSTRACT**	**18. NUMBER OF PAGES**	**19a. NAME OF RESPONSIBLE PERSON**
a. REPORT	**b. ABSTRACT**	**c. THIS PAGE**			Renu B. Rastogi
U	U	U	UU	54	**19b. TELEPHONE NUMBER** *(include area code)* (410) 436-7545

Blank

PREFACE

The work described in this report was authorized under contract no. W911SR-14-P-0022. The work was started in March 2014 and completed in March 2015.

The use of either trade or manufacturers' names in this report does not constitute an official endorsement of any commercial products. This report may not be cited for purposes of advertisement.

This report has been approved for public release.

Acknowledgment

The authors acknowledge Dr. A. Peter Snyder (retired U.S. Army Edgewood Chemical Biological Center) for his free technical discussions, editing, and guidance.

Blank

CONTENTS

FIGURES

HIGHLY RESOLVED SUB-TERAHERTZ VIBRATIONAL SPECTROSCOPY OF BIOLOGICAL MACROMOLECULES AND BACTERIA CELLS

1. INTRODUCTION

Sub-terahertz (sub-THz) spectroscopy has become recognized as a fast technique for sensing and detecting biological molecules and microorganisms. It is based on the interaction of terahertz (THz) radiation with internal molecular vibrations of low energy. In the literature, a majority of THz experimental data have been reported on frequencies above 1 THz and for relatively small biological molecules that are often prepared in crystalline form (*1*). Some progress (past 4–6 years) has been reported in the literature for detecting large biological molecules and microorganisms using sub-THz (below 1 THz) spectroscopy with improved sensitivity (*2*). Molecular dynamic (MD) simulations for relatively small molecular components correlate well with the experimental data (*3*).

Bacteria are very complex biological objects. Because of their small size and relatively low absorption coefficient, THz radiation propagates through the entire object, which allows the genetic material and proteins to contribute to the THz signature of individual bacteria or spores. In the past, transmission vibrational-mode intensities of 1–2% could be obtained when solid samples were characterized using a Fourier transform infrared (FTIR) spectrometer (IFS 66v; Bruker Daltonics; Bremen, Germany) with a moderate spectral resolution of 0.25 cm^{-1} (*2*). Raw transmission spectra and absorption coefficient data were calculated for the quantitative characterization of biological materials; however, discriminative capabilities needed to be improved. Observed spectroscopic features from biological cells and spores are caused by the interactions between THz radiation and biological macromolecules. These features can include combinations of low-energy vibrational modes or groups of modes at close frequencies (vibrational bands) within the molecular components of bacterial cells and spores, with a significant contribution from the DNA (*2, 3*). The entire mechanism of MDs is still not understood and needs to be studied. The suggested range of MD relaxation times (τ) for processes without biological molecular conformational change varies from approximately 1.5 to 650 ps in different studies (*4*, *5*).

The width of individual spectral lines and the intensity of resonance features observed in sub-THz spectroscopy are sensitive to the relaxation processes of atomic dynamics (displacements) within a macromolecule. Those relaxation processes determine the discriminative capabilities of sub-THz spectroscopy. Appropriate spectral resolution must be used in THz spectroscopy to be able to acquire qualitative as well as quantitative genetic information used to identify the characteristic signatures of biological objects that will, in turn, increase detection accuracy and selectivity. The narrow spectral lines are due to the existence of long-lasting dynamic processes. This was confirmed by the relaxation dynamics of side chains in macromolecules that were observed using time-resolved fluorescence experiments (*6*), which required the application of highly resolved vibrational THz spectroscopy. The majority of available THz spectroscopy systems do not have the high spectral resolution that is required to observe narrow-width spectral lines.

Experimental measurements with good spectral resolutions have been demonstrated (*7*, *8*) in which intense and narrow spectral features were observed from biological molecules and bacteria with spectral widths between 0.05 and 0.2 cm^{-1}. These features were not evident in previous experimental measurements that used a spectral resolution of 0.25 cm^{-1}. These findings suggested the coexistence of diverse relaxation dynamics mechanisms that are relevant to the sub-THz frequency region (*9*). Multiple intense and specific resonance signatures may provide a way for the development of reliable discriminative capabilities using the new sub-THz frequency-domain spectroscopy described herein. This was not possible using the methods discussed in the previous literature studies. The controversies found in the relatively young sub-THz spectroscopy field were due to experimental problems, such as poor spectral resolution and sample preparation techniques that were not adequate for the problem.

The Vibratess (Charlottesville, VA) sub-THz spectrometer is a continuous-wave, frequency-domain spectroscopic THz instrument with imaging capability. The detector operates at room temperature without the need for cryogenic cooling. Frequency transmission spectra were obtained in the sub-THz region between 315 and 480 GHz for macromolecules and biological species. Due to the high sensitivity, good spectral resolution, and a spatial resolution, the spectroscopic instrument allows for the observation of intense and narrow spectral resonances in transmission and absorption spectra for nanogram amounts of samples obtained from biological materials with spectral line widths as narrow as ~0.1 cm^{-1}. Experimental spectra from the new sub-THz spectrometer, obtained using nanogram quantities of biological macromolecules and biological cells and spores, were compared to the MD simulations.

The majority of THz systems that are commercially available use the time-domain approach. Some disadvantages of this approach are: (1) fast Fourier transform (FFT) is a powerful technique, but there are limitations on the use of FFT with discrete data points (not continuous function); (2) multiple frequencies radiate onto the sample, which leads to unreliable absorptions and measurements (e.g., cross-vibrations); and (3) collection of limited data points will force averaging of absorption peaks.

The frequency-domain THz system used in this study has the following advantages: (1) new and reliable THz signature, (2) better resolution with frequency-domain THz signatures, and (3) simulation that can be used to easily explain any single THz peak of interest.

2. EXPERIMENTAL SETUP

2.1 New Sub-THz System

The new Vibratess sub-THz system (VsTHz; Figure 1) has several advantages over the commercial systems available at the time of this study (e.g., Bruker IFS 66v). The VsTHz system does not require milligram quantities of biological material, a liquid helium cooled detector, operating under vacuum, or purging with dry gas. Although some specificity was observed in different bacterial spectra using the Bruker IFS 66v instrument, the absorption peak intensities for *Bacillus subtilis* and *Escherichia coli* were rather close. This suggests that the

spectral resolution of 0.25 cm^{-1} did not provide a sufficient level of discrimination. Better spectral resolution is required for better discrimination and clear specificity. Other important characteristics of a sub-THz system are small sample size requirements, a simple sample-preparation procedure, room-temperature operation, good reproducibility, and user-friendly operation for wide-spread adoption of a new system.

The new VsTHz system was developed with improved spectral resolution, which was close to 1 GHz (0.03 cm^{-1}). THz systems described in previous literature lacked spectral resolution. The VsTHz system operates in a frequency domain at room temperature and with local enhancement of the electromagnetic field; therefore, coupling of the THz radiation with the sample biomaterials was increased (*8*, *10–14*).

The VsTHz system operates in a frequency range between 315 and 480 GHz, with an average output power of ~0.2 mW. It includes a sub-THz electronically tunable source that is based on Schottky frequency multipliers (Virginia Diodes, Inc. [VDI]; Charlottesville, VA) and a submicron, precision motorized stage to provide three-dimensional (3D) scanning capability for a detector subsystem, relative to a 6 mm wide, multichannel sample chip holder (Figure 2). The detector system has a microdetector (Schottky diode from VDI) with a replaceable beam-lead microprobe (Lichtenberger Consulting; Charlottesville, VA) and a planar microdetector circuit (*15*), which is mounted in a custom microwave guide housing.

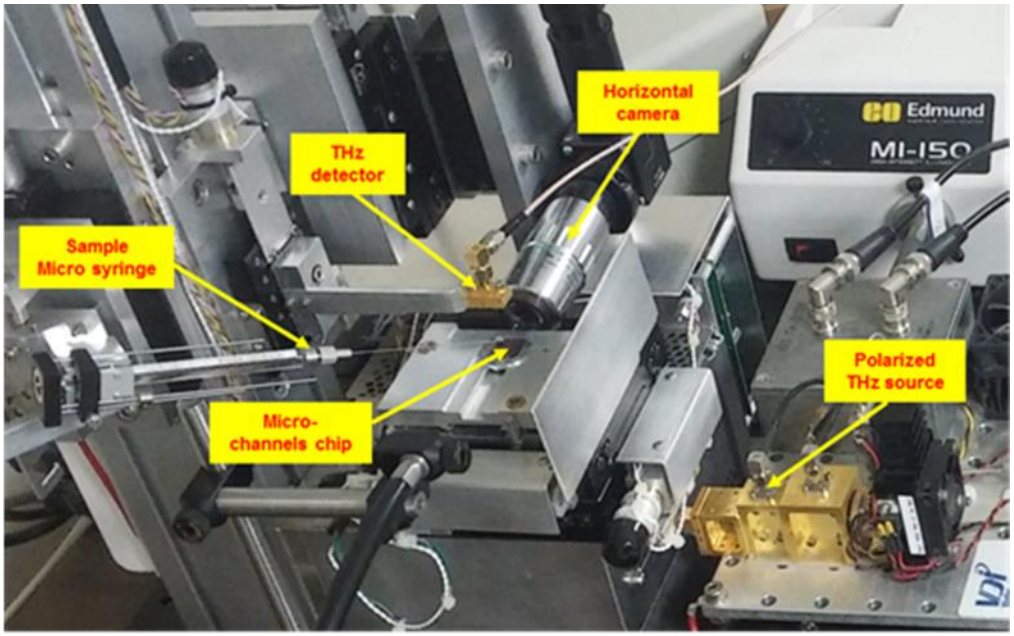

Figure 1. Vibratess spectroscopic sensor prototype. Micro-THz detector, microchannels sample chip holder, and objective for optical visualization (horizontal camera).

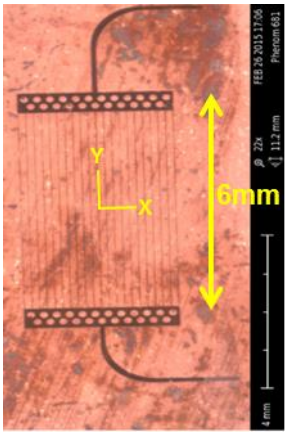

Figure 2. Microchannels (along the *y* axis from –3000 to 3000 μm) sample chip (6 mm wide).

The sample chip holder (Figure 2) is constructed of an array of microchannels in a gold or copper layer on a substrate. The substrate is any material with a low absorption coefficient and a low refractive index that is in the THz range. This configuration generates the edge effect, which is necessary for enhancement of the electromagnetic field of the THz radiation and provides regions for holding biological materials. The substrate material we used was polymethylmethacrylate with channel widths of 5–20 μm. The thickness of the gold layer (2–5 μm) determines the channel depth. A high-magnification optical-imaging system with a long working-distance objective allows accurate positioning of components. The waveguide and microdetector circuit were designed using a high-frequency structure simulator to separate THz radiation from a direct current Schottky diode signal. Spatial resolution is better than 200 μm and is restricted by the opening size of the commercially available microdetector waveguide (150 × 200 μm^2). In the future, smaller microdetector waveguides can be used to increase the spatial resolution (lower than 200 μm).

2.2 Experimental Procedure

Care was taken to prevent the system from overheating and to ensure the temperature stabilization of the microchannel chip and protein samples under investigation. We took steps to minimize the heat from the illumination source and ensured that the temperature in the room was controlled at 24–25.5 °C during measurements.

The minimum possible amount of sample material in a channel used for interrogation was 0.05 ng in an area of 10 × 200 μm, with a channel depth of 3 μm. A protein solution droplet size of 0.2 μL, with concentration of 0.25 mg/mL, yielded enough solution to spread on an area ~1 × 2 mm^2. This was more than the amount required to provide high sensitivity for THz characterization. It is crucial to ensure that the sample material layer is very thin. In our example, the dried layer thickness during the sample spectrum scan was ~2.5 μm, which was slightly less than the channel depth. A thicker sample layer (>3 μm) containing water will have a significantly higher dielectric constant in our frequency range as compared with air and plastic. This will modify the optical path for radiation through the sample chip as compared with the background of empty channels, which will result in artificial values of the calculated transmission above 1. In addition, a very thin substrate (only 25 μm thick) bends under the

weight of the sample material solution, which also causes poor stability and reproducibility. In our case, the reproducible results were obtained after ~2 h of material drying. Additional improvements are needed to reduce this waiting time from hours to several minutes after sample solution deposition on the chip.

2.2.1 Sample Preparation and Deposit

For this study, a micropipette was used to deliver a 0.1–0.3 μL droplet of biological sample in liquid suspension (80% water and 20% methanol) on a preselected spot on the sample chip (array of microchannels) in the sample holder. Within a minute, the droplet on top of the sample chip shrank quickly in size and then evaporated completely. The microdetector probe was positioned several microns above the droplet's spot on the sample chip. Only ~20 ng of biomaterial is required for the VsTHz system, as compared with the milligram sample size required for other THz systems that are mentioned in the literature.

2.2.2 Data Collection and Measurements

Measurements and data collection were performed 10 min after the droplet was deposited and the sample was dried. The acquired data consisted of an array containing the frequency-dependent signal and other pertinent metadata including data, time, and the 3D probe coordinates. A spectral resolution >1 GHz was achieved, along with high sensitivity. A typical signal-to-noise ratio obtained was ~103 (depending on frequency) at room temperature (without the requirement for air evacuation or purging with dry nitrogen).

2.2.3 Characterization of the Sub-THz System

Figure 3 shows the periodicity of the transmitted signal at a frequency of 15.5 cm^{-1} as the probe was scanned across the sample chip microchannels from a blank run (no biological sample deposited). As expected, it showed the same periodicity as the array itself, although the data was slightly offset in the *x* direction from the channels.

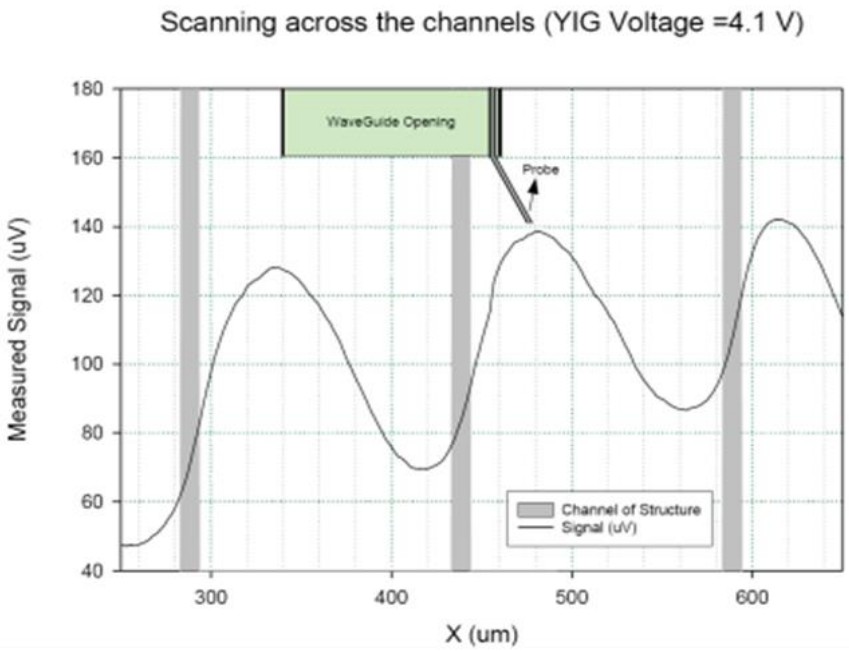

Figure 3. Periodicity of a THz signal (measured signal in microvolts, gray line) in the direction (*x* in micrometers from the center of the sample chip [Figure 2]) perpendicular to the microchannels (gray bar).

Figure 4 shows the transmitted signal at a frequency of 15.5 cm^{-1} of a sample of *B. subtilis* at four microchannel *y*-axis values (–250, –300, –350, –400 μm [Figure 2]) as the probe was scanned across the sample chip microchannels (in the *x*-axis direction). Figure 2 shows the microchannel *x* and *y* directions. The sample was located between –450 and 150 μm on the microchannel *x* axis, but a longer scan was used, and the observed transmission was close to 1 as the probe was scanned across empty microchannels (no biological sample). Transmission was reduced to about 60% in area as the probe was scanned across microchannels with biological sample. The actual reduction depended on the amount of biological material in each channel.

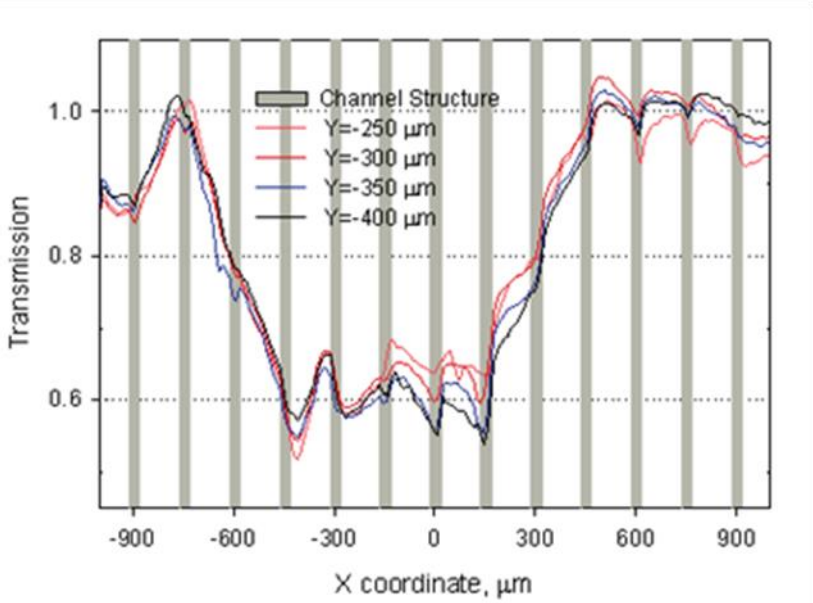

Figure 4. Transmission scan across channels with *B. subtilis* cell material.

3. THZ MOLECULAR DYNAMIC (MD) SIMULATION OF BIOLOGICAL MATERIALS

In a parallel study, a computational modeling technique was developed to simulate vibrational spectra of proteins using the energy minimization, normal mode analysis, and MD approaches. The MD simulations were performed using the assisted model building with energy refinement (AMBER) simulation program package (University of California; San Francisco, CA) as described by Alijabbari et al. (*3*), with a modified procedure to improve the convergence of modeling results for proteins.

3.1 Insulin MD Simulation

To model the insulin molecule, it was necessary to correctly choose an insulin crystal structure file from the protein data bank (PDB) that most closely corresponded to an experimental material used in our absorption measurements. The PDB database contains 436 structures related to human insulin. The experimental material (Sigma-Aldrich Corporation [St. Louis, MO], catalog no. I0908 SIGMA) consisted of a mix of insulin and Zn^{2+} ions (Figure 5A–C). It is known that three insulin molecules are able to form a stable complex with Zn^{2+} ion in the center (*1*) as shown in Figure 5A (*16*).

The PDB file (3W7Z) was used for MD simulation of the entire complex. The crystalline structure of this complex is shown in Figure 5A. Other structures of insulin can be simpler and contain only one insulin molecule that consists of two chains with disulfide bridges, as shown in Figure 5B,C. Two different PDB files were used as starting points to simulate a single insulin molecule—one of them was PDB file 3W7Z, which uses Zn^{2+} ions to stabilize the structure, and the second was PDB file 3I3Z. This file (3I3Z), which represents only one

molecule, was chosen because it contains the atomic coordinates of human insulin crystallized without Zn^{2+} ions.

As shown in Figure 5A, three insulin molecules formed a stable complex with the Zn^{2+} ion (green) in the center through interaction between Zn^{2+}, water molecules, and histidine residues (data from 3W7Z PDB file). In Figure 5B, two chains of insulin molecules with one intra- and two intermolecular disulfide bridges (yellow). Insulin was crystallized with Zn^{2+} ions (data from 3W7Z PDB file). In Figure 5C, in contrast with the molecule in Figure 5B, the molecule was crystallized without Zn^{2+} ions (data from 3I3Z PDB file). Atom positions were slightly different but similar in configuration.

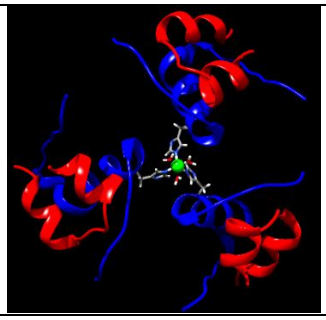	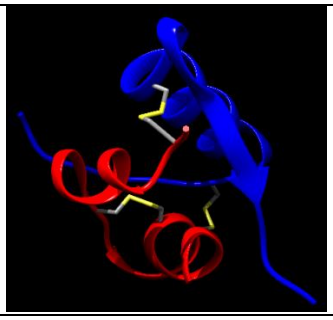	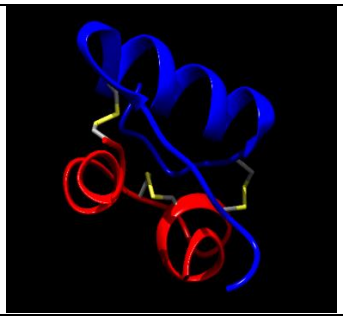
A Three insulin molecules form a stable complex with the Zn^{2+} ion (green) in the center. The complex is formed through interaction between Zn^{2+}, water molecules, and histidine residues (data from 3W7Z PDB file).	B Two chains of insulin molecules with one intra- and two intermolecular disulfide bridges (yellow). Insulin was crystallized with Zn^{2+} ions (data from 3W7Z PDB file).	C In contrast with a molecule in Figure 5B, this molecule was crystallized without Zn^{2+} ions (data from 3I3Z PDB file). Atom positions are slightly different but similar in configuration.

Figure 5. Three insulin molecules.

3.2 Lysozyme MD Simulation

There are several 3D molecular structures for lysozyme available in the PDB, including 1BWH, 1LYS, and 4QEQ PDB structures determined from X-ray analysis. It is important to choose the best structure that most closely correlates with the real structure of purchased lysozyme for MD simulations and analysis. In previous literature studies, the structure 1BWH was found to have a low resolution. The 4QEQ PDB structure has been obtained only recently. The quality of X-ray crystal structures of 4QEQ and 1LYS PDB can be found at the PDB website for lysozyme files (*17, 18*).

The information provided in this section was based on the global validation metrics for the 4QEQ and 1LYS lysozyme PDB files. According to this global validation metric criteria, the 4QEQ structure has better Ramachandran (*3*) and Sidechain outlier scores, which

means that the structure of 4QEQ is of better quality. Several MD simulations were conducted using the 1BWH PDB file. This included three different initial random atomic velocities and total energy (E_{TOT}) of a molecular system at room temperature (293 K) and at an elevated temperature of 298 K.

4. DISCUSSION

The ability to quickly and reliably discriminate between different bacterial species, toxins, and proteins using sub-THz spectroscopy would provide significant benefits to the medical first responders and soldiers. For example, in the medical field, it would enable a faster and more-tailored treatment for a patient or affected area once a bacterial organism or toxin is identified as the cause of an infection, spillage, release, and so on.

To demonstrate the capabilities of the VsTHz spectrometer, and to fully understand the basic fundamentals of THz absorption by biomaterials, the study started with commonly used proteins that had peptide deformylase structures in the public database before beginning a THz study of bacterial cells and some of their molecular components (DNA and thioredoxin). Extensive experimental characterization and MD simulations of THz spectroscopic signatures were conducted using human insulin protein and chicken egg-white lysozyme protein.

Proteins with different structures will absorb and vibrate in response to light of different frequencies. A protein can be considered like a tree with different size leaves and branches; as air passes over the tree, the leaves and branches vibrate and slightly rotate at different frequencies. Protein end groups are like the leaves and amino acids are like the branches of the tree.

4.1 Insulin THz Study

4.1.1 Insulin THz Experimental Spectra

The human insulin protein (I0908, molecular weight ~5800 Da) was purchased from Sigma-Aldrich (http://www.sigmaaldrich.com/catalog/product/sigma/i0908?lang=en&region=US). Human insulin is a two-chain polypeptide hormone produced by the β-cells of pancreatic islets. The α and β chains are joined by two interchain disulfide bonds. The α chain contains an intrachain disulfide bond. Insulin regulates the cellular uptake, utilization, and storage of glucose, amino acids, and fatty acids and inhibits the breakdown of glycogen, protein, and fat.

The human insulin protein we obtained was actually a mixture of insulin and Zn^{2+} ions. Through direct communication with Sigma-Aldrich technical support, it was found that there was no available PDB file that could be used to characterize the 3D structure of Sigma-Aldrich insulin.

The transmission spectra shown in Figure 6 was obtained by following the experimental setup, sample preparation, and data collection procedures discussed in Sections 2.2 to 2.2.2. Figure 6 shows the transmission change over time while the material fully dried (80, 130, and 250 min). In this example, the sample material was diluted to very low concentration of 0.25 mg/mL to slow the drying process. The data show that the position of all transmission minima on the frequency scale was preserved, although the absolute value of transmission was changing.

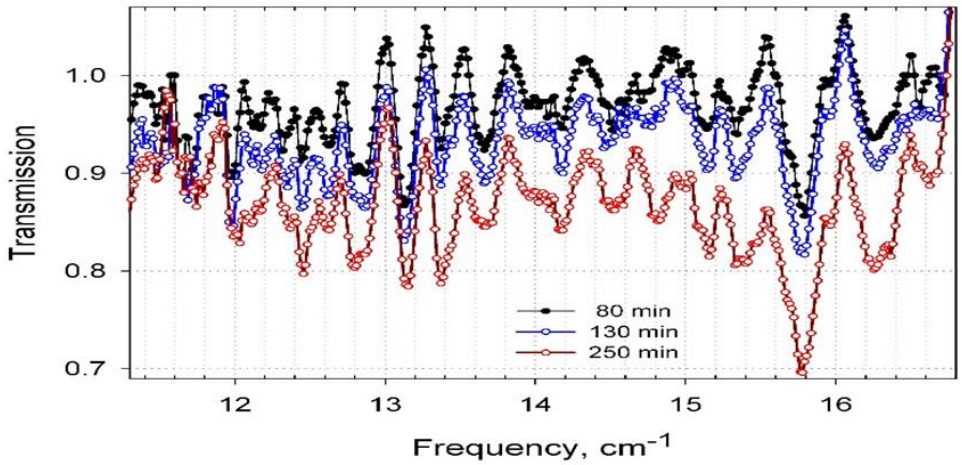

Figure 6. Transmission change depending on drying time (insulin concentration of 0.25 mg/mL in 50% ethanol and droplet size ~1 μL).

Transmission spectra were recalculated to absorbance, $A = -\log(\check{T})$, where $\check{T}$ is transmission. Figure 7 compares the absorbance of dried sample (transmission at 250 min, the red line plot on Figure 6) with the averaged results from measurements at different spots on a chip. Once again, the frequencies of most transmission minima were reproduced. The red spectra shown in Figures 6 and 7 are the same; Figure 6 is shown in transmission scale, and Figure 7 is shown in absorbance scale. The red spectrum in Figure 7 was chosen over the average spectrum of all spots for comparison with MD simulations because it was more reliable and had stronger maximum absorptions.

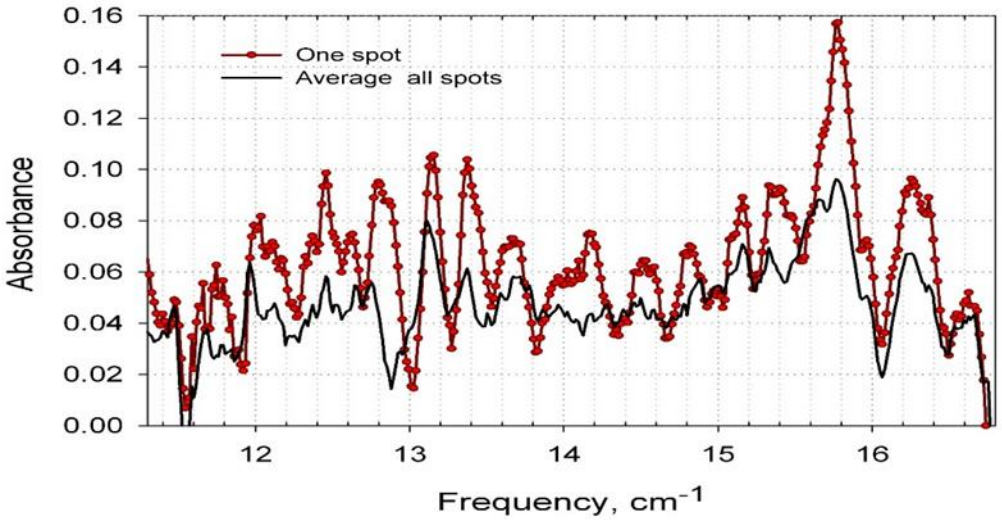

Figure 7. Variability of experimental spectra that depends on the radiation intensity variation in different channels and spots on a microchip. (Insulin concentration of 0.25 mg/mL in 50% ethyl alcohol and droplet size of 0.3 μL).

Figure 8 demonstrates the absorbance spectra from thicker sample layers. In this case, the drying process required several days to be completed. The results were less reliable because the background and sample measurements were conducted on different days to allow sufficient time for the material to fully dry.

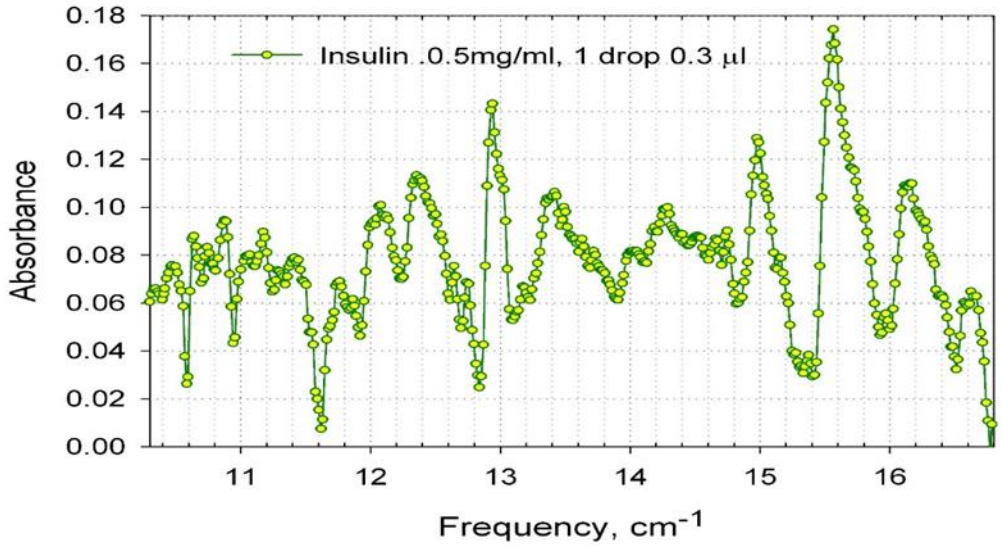

Figure 8. Measured absorbance spectrum from thick insulin sample after drying for several days. (Insulin concentration of 0.5 mg/mL and droplet size of 0.3 μL).

As shown in Figure 8, the most-important result was that the dominant absorption peak was identified at frequencies 15.5–15.8 cm^{-1}. The most-reliable data, shown by the red lines in Figures 6 and 7, were further used for comparison with results from MD simulations.

4.1.2 Insulin THz MD Simulations

To model the insulin molecule, it was necessary to choose a PDB insulin crystal structure that most closely corresponded to an experimental material used in our absorption measurements. The PDB file (3W7Z) contained information about the complex of three insulin molecules with Zn^{2+} ions; therefore, it was used for the MD simulation of the entire complex. The crystalline structure of this complex is shown in Figure 5A. The material in the experiment was amorphous and did not have the crystalline structure shown in Figure 5A, which was specifically built for X-ray analysis. The unit in this amorphous material can be simpler and may contain only one insulin molecule, which consists of two chains with disulfide bridges, as shown in Figures 5B and 5C. Two different PDB files were used as a starting point to simulate a single insulin molecule: PDB file 3W7Z, which used Zn^{2+} ions to stabilize the structure, and PDB file 3I3Z. The PDB file 3I3Z, which represents only one molecule, was chosen because it contains atomic coordinates of human insulin crystallized without Zn^{2+} ions.

To characterize the theoretical spectrum of insulin, and to better analyze and understand the experimental spectra, we conducted multiple simulations with two different goals. The first goal was to estimate the variability of the spectra due to the difference of initial atomic coordinates taken from crystal structures by modeling one insulin molecule. For this purpose, we modeled single insulin molecules that were crystallized with Zn^{2+} ions (3W7Z PDB file) and without Zn^{2+} (3I3Z PDB file).

The second goal was to estimate the effect of weak intermolecular bonds between insulin molecules by modeling a complex of three insulin molecules together with Zn^{2+} ions. This question was addressed by comparing the simulation results obtained for a single molecule with those of the complex taken from the same PDB file, 3W7Z.

MD simulations were performed, and absorption coefficients were found using the procedures described in Section 3.1. A detailed description of the Vibratess protocol approach for MD simulation using the AMBER program can be found in a study done by Globus et al. (*2*). We simulated a complex containing a biomolecule and an 8 Å shell of TIP3P water. In the preparation of this complex, a constant number, volume, and temperature (NVT) ensemble was used to raise the temperature to 293 K.

The system was heated for ~16 ps, and the protein atoms were restrained using a 10 kcal/mol/$Å^2$ force constant. During this heating process, the bonds involving hydrogen were fixed. Constant pressure periodic boundary conditions were used to scale the system volume during 100 ps to reach a density of ~1 g/cm^3. In these procedures, a 10 Å real-space cutoff was used with a 2 fs integration time step. After the system attained the selected values of temperature and density, random velocities from the Maxwellian distribution were assigned to all atoms, followed by another equilibration step; then a constant number, pressure, and temperature (NPT) ensemble was used for further energy minimization. After equilibration, a 600 ps

production run was performed in a constant number, volume, and energy (NVE) ensemble to avoid undesirable effects on atomic motions because of coupling to an external thermal bath. During the simulation, the coordinates of all atoms of the system were recorded every 20 fs for the entire production run. Atomic trajectories collected in MD simulations were converted to the covariance matrix of atomic random displacements, $\langle R_i R_k \rangle$. The force-field matrix is found in a quasi-harmonic approximation using the relation between the covariance matrix and the inverse of the force-constant matrix ($\langle R_i R_k \rangle = k_B T [F - 1]_{ik}$), where R is the random displacement value between atom i and atom k, T is temperature, and F is a force constant (*3*, *4*). Diagonalization of the F matrix gives eigenfrequencies (normal mode frequencies) and eigenvectors (displacement vectors–normal modes).

Using atomic trajectories from the constant energy and volume MD simulations, insulin sub-THz vibrational spectra and absorption coefficients were calculated in a quasi-harmonic approximation. The absorption coefficient spectra $\alpha(\nu)$, as a function of the frequency (ν), can be calculated through the relationship between α and the imaginary part of dielectric permittivity (*5*)

$$\alpha(\nu) = W\nu^2 \sum_k \frac{S_k}{(\nu^2 - \nu_k^2)^2 + W^2\nu^2} \quad (1)$$

where ν_k is the normal mode frequency, calculated by diagonalization of the force-constant matrix, and S_k is the oscillator strengths computed for all vibrational modes, *k*. The spectral line width, $W = 0.12$ cm^{-1}, which is close to the width of spectral features observed in experiments with the Vibratess spectrometer, was used for all of our vibrational-mode simulations in sub-THz range.

Better simulation convergence and improved consistency between simulated vibrational frequencies and experimental data were obtained using a new procedure for averaging mass-weighted covariance matrices of atomic trajectories in MD simulations (*2*). Averaging of only six matrices gave consistent results. The overall stability of protein MDs was estimated using a comparison of two spectra that were calculated with a covariance matrix from an entire production run and from an averaged covariance matrix (*3*, *20–22*).

Figures 9–12 show the MD simulation results compared with the experimental spectrum (red curve in Figure 7). The MD simulations also confirmed that THz absorption peaks have a peak width of approximately 0.2 cm^{-1}. This means that the proper THz system should have a THz resolution of at least 0.01 cm^{-1} (20 points per THz absorption peak or higher). Better resolution requires a longer time for collecting data and does not provide any additional information.

Figure 9 shows the experimental THz spectrum of insulin, compared with the MD simulation THz spectrum obtained for a single insulin molecule using the 3W7Z PDB file. There was good correlation with the most-prominent experimental THz absorption peak (15.5–16.2 cm^{-1}) when one insulin molecule, crystallized with Zn^{2+}, was modeled. The vertical green lines in Figure 9 represent the THz absorption peaks found in the experimental and

modeling spectra (six matching peaks). The most-prominent MD simulation peak is located at ~15.9 cm^{-1}. The most-prominent experimental THz spectrum peak is located at ~15.8 cm^{-1}.

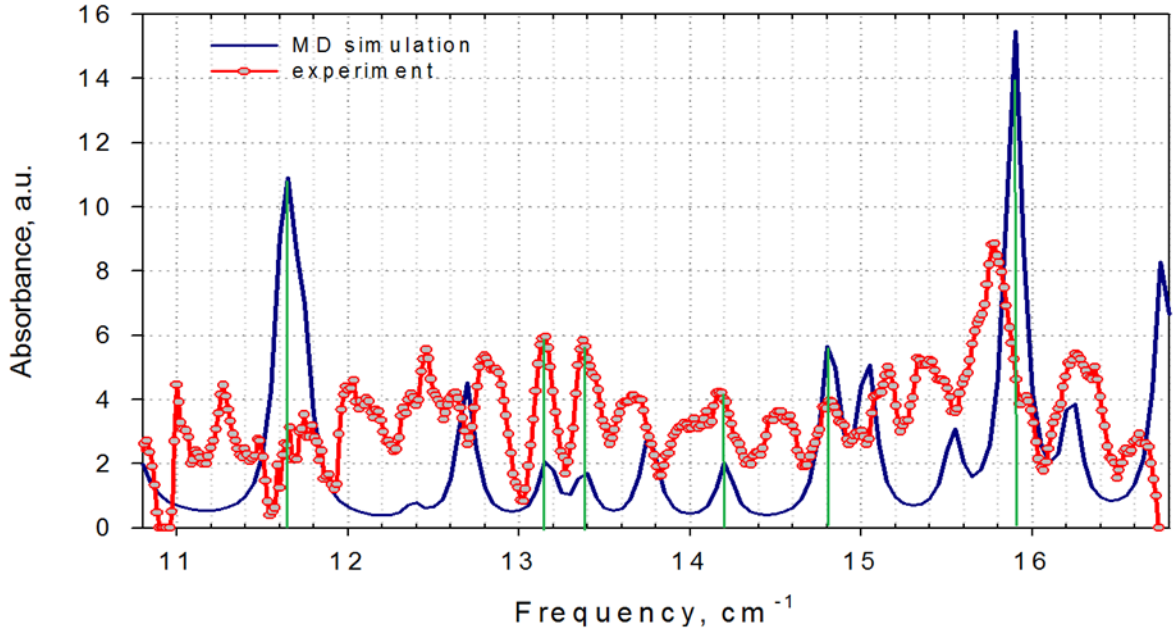

Figure 9. Insulin experimental THz spectrum compared with the MD simulation THz spectrum for a single insulin molecule using the 3W7Z PDB file with Zn^{2+}.

Figure 10 shows the experimental THz spectrum compared with the MD simulation THz spectrum using a single insulin molecule from the 3I3Z PDB file. The MD simulation THz spectrum that was based on the 3I3Z PDB structure crystallized without Zn^{2+}; however, the most-prominent peak is located at ~14.6 cm^{-1}, which is not in agreement with the experimental THz spectrum. The vertical blue lines in Figure 10 represent the THz absorption peaks found in experimental and modeling spectra (five matching peaks). The most-prominent experimental THz spectrum peak is located at ~15.8 cm^{-1}.

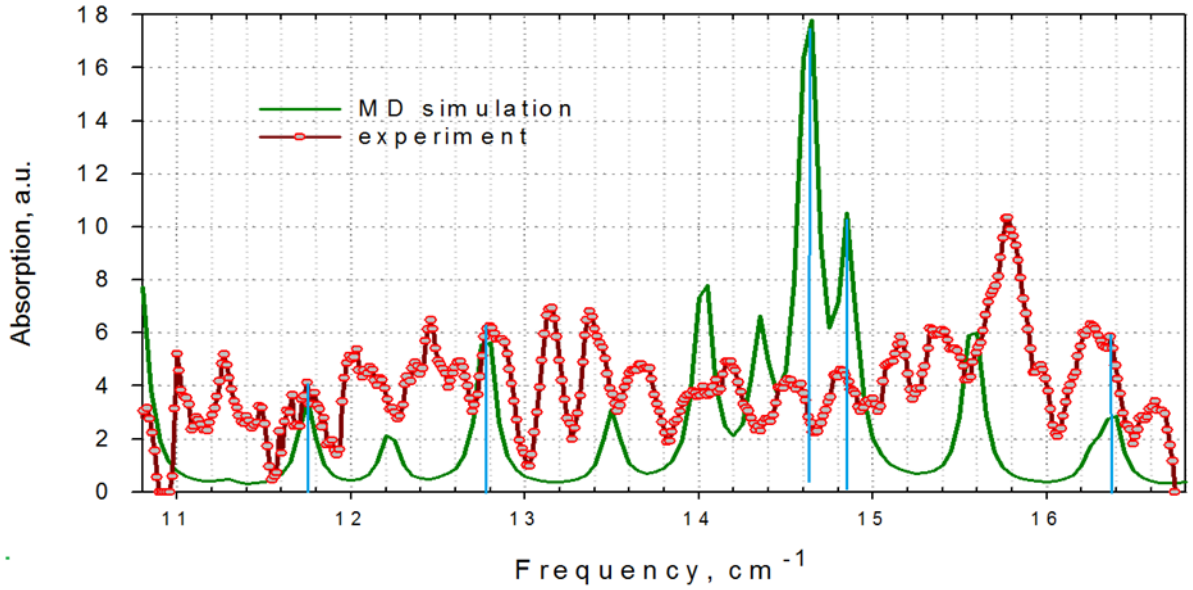

Figure 10. Experimental THz spectrum compared with the MD simulation THz spectrum for a single insulin molecule from the 3I3Z PDB file without Zn^{2+}.

Figure 11 shows the experimental THz spectrum compared with the MD simulation THz spectrum obtained using the complex of three insulin molecules and a Zn^{2+} ion. The MD THz spectrum simulated using the 3W7Z PDB structure for a complex of three molecules and a Zn^{2+} ion (Figure 5A) showed good correlation with experimental absorption peaks at frequencies 11.4, 12.2, 14.2, 16.3, and 16.6 cm^{-1}, as shown in Figure 11. The vertical green lines in Figure 11 represent the THz absorption peaks found in experimental and modeling spectra (eight matching peaks). There are three most-prominent MD simulation THz peaks located at ~11.2, 13.2, and 14.2 cm^{-1}. The most-prominent experimental THz spectrum peak is located at ~15.8 cm^{-1}.

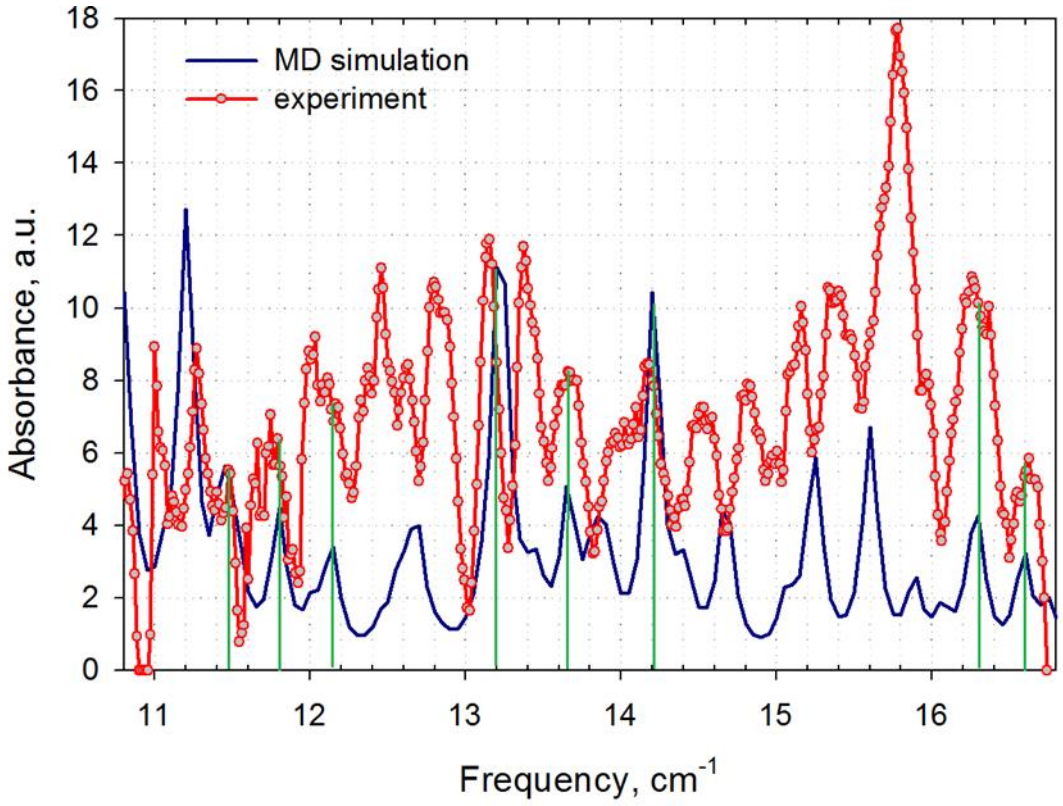

Figure 11. Experimental spectrum compared with the MD simulation THz spectrum for the complex of three insulin molecules and Zn^{2+} ion PDB file.

Figures 9 and 11 show results with better fits to the experimental THz spectra as compared with Figure 10. Based on the correlations (vertical lines) shown in Figures 9 and 11, it can be assumed that the experimental material might be a mixture of two components: (1) a single insulin molecule and (2) a complex of three insulin molecules crystallized with Zn^{2+}. A combined MD simulation THz spectrum was calculated from the two 3W7Z PDB structure MD simulations where two spectra were taken with 1:1 ratios. This new, combined spectrum (Figure 12) had an improved correspondence as compared with the experimental data.

Figure 12 shows the experimental THz spectrum as compared with the average MD simulation. The THz spectra were obtained from a single insulin molecule MD simulation and from the complex of three insulin molecules MD simulation crystallized with a Zn^{2+} ion (data 3W7Z PDB file). The vertical green lines in Figure 12 represent the THz absorption peaks found in the experimental and modeling spectra (nine matching peaks).

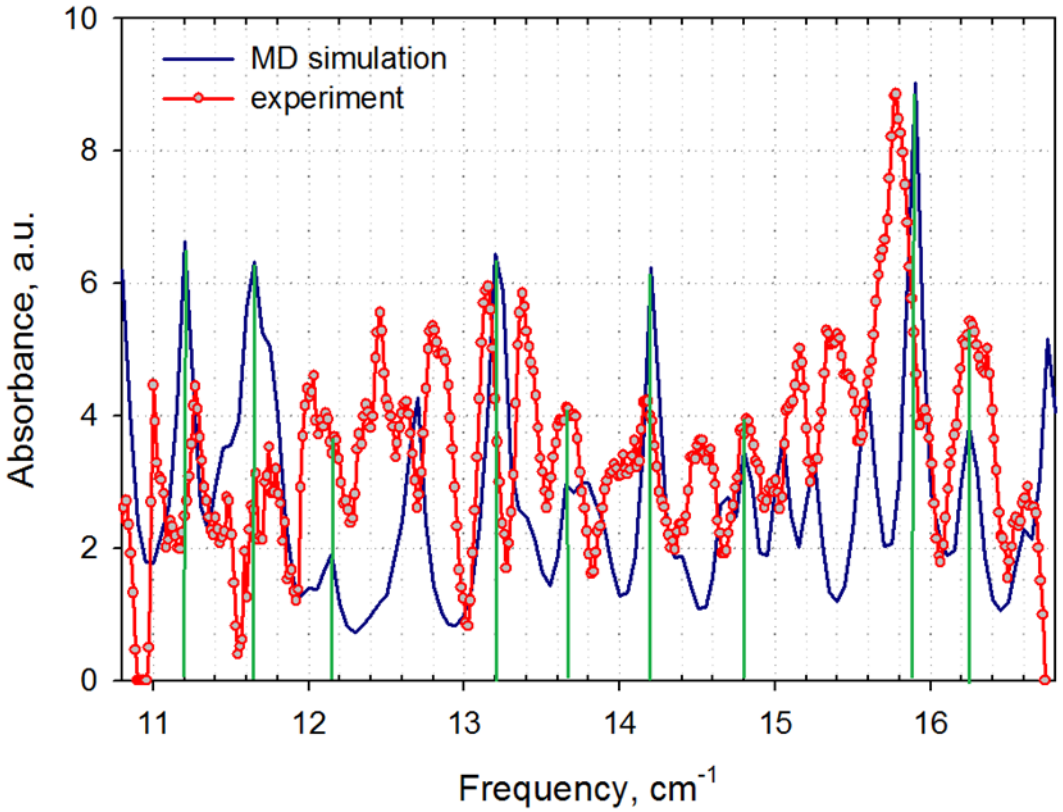

Figure 12. Insulin experimental THz spectrum compared with that of the average MD simulation. The vertical green lines represent the THz absorption peaks found in experimental and modeling spectra (nine matching peaks).

Results from the experimental THz spectrum and those from various MD simulations on human insulin in the sub-THz frequency range indicate that the origin of the vibrational modes is heterogeneous; in other words, it is a combination of multiple structures and ions.

4.2 Lysozyme THz Study

4.2.1 Lysozyme THz Experimental Spectra

Lysozyme is a small, globular protein composed of 129 amino acid residues. Lysozyme is able to damage bacterial cell walls by catalyzing the hydrolysis of peptidoglycans (found in the cell walls of bacteria, especially Gram-positive bacteria) and hydrolyzing the glycosidic bond that connects *N*-acetylmuramic acid with the fourth carbon atom of *N*-acetylglucosamine. Lysozyme is widely used in the enzymatic lysis of microbial cells (*23*, *24*).

The lysozyme material that was used for experimental characterization was purchased from Sigma-Aldrich and contained L6876 lyophilized powder and protein ≥90% (≥40,000 units/mg of protein). The lysozyme sample with a concentration of 5 mg/mL in distilled water was prepared at the U.S. Army Edgewood Chemical Biological Center.

The procedure that was used for experimental characterization was basically the same as that used for insulin and presented in Section 3.1. The previously used conventional light source that caused biosample material heating during measurements was substituted with the light-emitting diode base source.

Material with an initial concentration of 5 mg/mL was diluted to a concentration of 0.83 mg/mL with distilled water and mixed 1:1 with ethyl alcohol. Samples with the initial and diluted concentrations were both characterized.

Figure 13 shows the background THz spectral measurements at three different locations on the microchannels sample chip (as depicted in Figure 2) but very close together (*x*-axis locations were –448.55, –449.30, and –449.98 μm). These results showed good reproducibility between the three background THz spectral measurements (red, blue, and green lines) and the average spectrum (black) before the lysozyme sample was deposited.

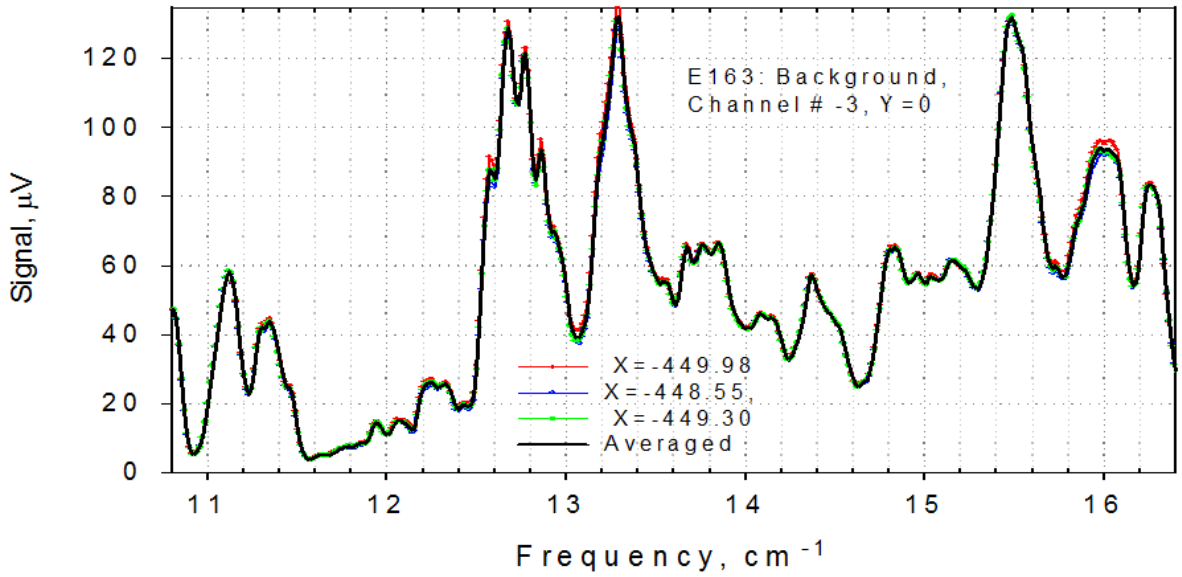

Figure 13. Reproducibility and variability of independent, background spectral measurements in the same position (sample chip microchannel [Figure 2] *x*-axis locations were –448.55, –449.30, and –449.98 μm) before the lysozyme sample was deposited.

Figure 14 shows the comparison between the average background THz spectrum (black line in Figure 13) and the chicken egg-white lysozyme THz spectrum (blue line) produced after the lysozyme sample was deposited. The signal intensity difference between the black and blue lines represents the absolute absorption.

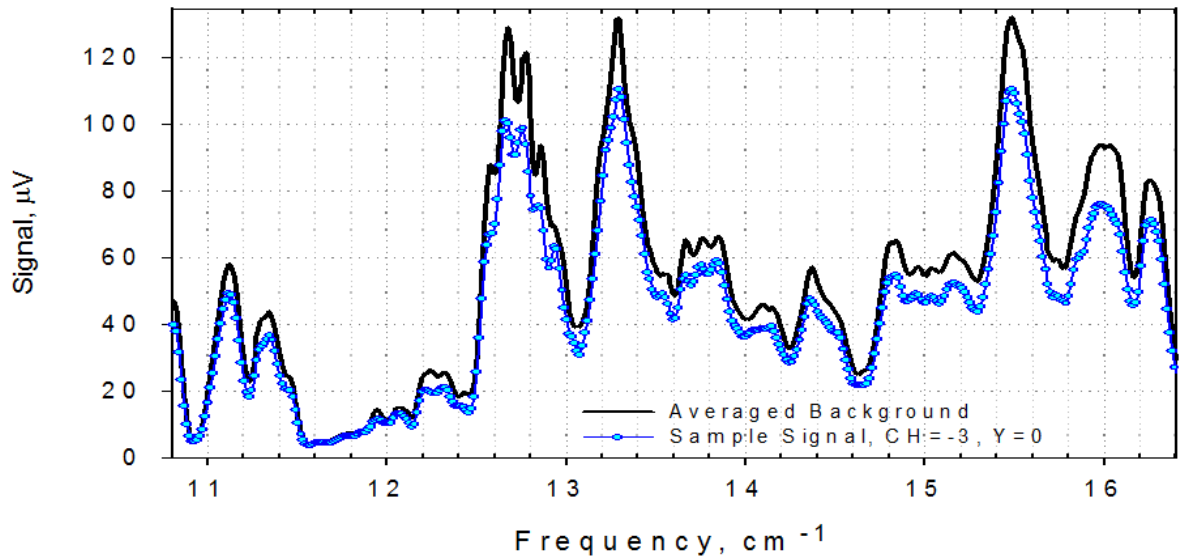

Figure 14. Comparison between average background spectrum and chicken egg-white lysozyme protein spectrum.

Figure 15 shows the experimental variability of the lysozyme transmission spectra at three very close locations on the microchannels sample chip (Figure 2); *x*-axis locations were –448.18, –449.53, and –449.75 µm, which are shown as blue, red, and green lines, respectively. The black THz spectrum represents the average of the three lysozyme transmission spectra. The three lysozyme transmission spectra were produced using the average background THz spectrum (black line in Figure 13). Note that the experimental THz spectral features (positions of local maximums and minimums) on the *x* axis (frequency) are reproducible, at better than 0.02 cm^{-1}. The reproducibility of the spectral features positions (local maximums and minimums) on the frequency *x* axis (Figure 15) was good at >0.02 cm^{-1}.

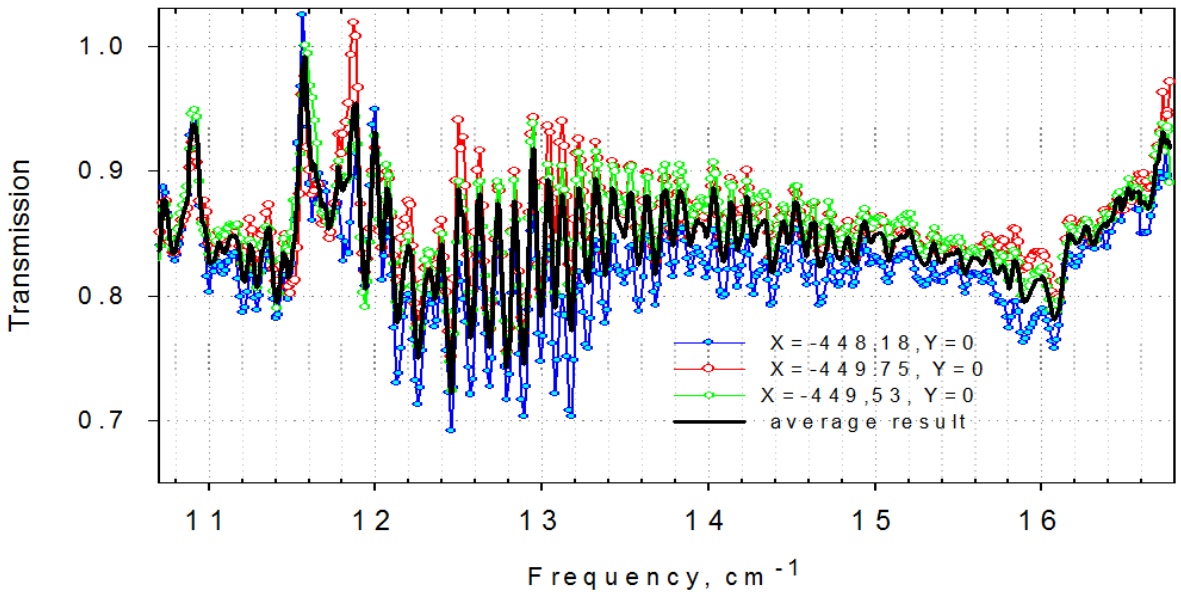

Figure 15. Variability of lysozyme transmission spectra at three very close locations on the microchannels sample chip (Figure 2); *x*-axis locations were –448.18, –449.53, and –449.75 μm. The black THz spectrum represents the average of the three lysozyme transmission spectra.

Figure 16 shows the change in the THz absorbance spectra based on the amount of sample material that was deposited on the same spot in the sample chip microchannel. Frequencies of all maxima and minima were reproduced extremely accurately, but the absolute values were different and did not follow Beer's law. This can be understood because the amount of sample material analyzed was restricted by the height of the sample chip holder microchannel.

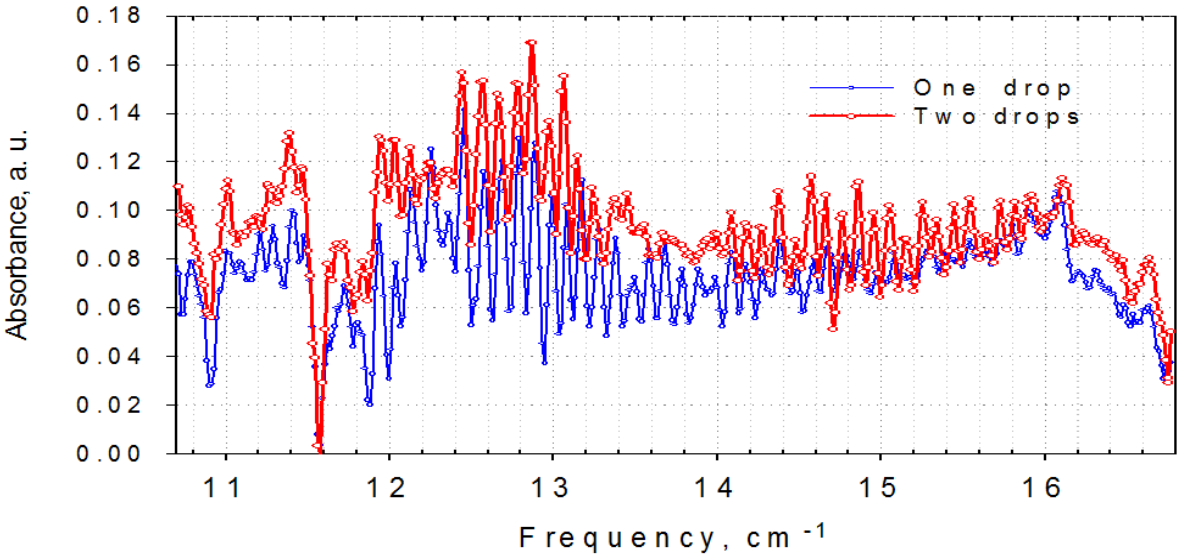

Figure 16. Lysozyme THz absorbance spectra for different amounts of material. Frequencies of all maxima and minima are reproduced accurately.

Figure 17 shows that the larger concentrations (blue and brown lines, 5 and 0.41 mg/mL, respectively) did not reduce the transmission on the same location (y = 0 μm). However, the transmission spectra had slight variation at different locations on the microchannels (y = 0 and –150 μm, blue and brown, respectively). Spectral variations are due to the variations in the sample and how the sample spread over different microchannels. THz measurements at different locations or spots on the microchannels chip play a big role in the measured THz spectra, as shown by the blue spectrum at a location y = 0 μm on the y axis as compared with the brown spectrum at a location y = –150 μm on the y axis. Future studies will examine the role of sample spread and amount on the measured THz spectra to find the optimal experimental settings. The transmission spectra in Figure 17 need to be converted to absorbance spectrum (Figure 18) to be further compared with the THz MD simulations. Figure 18 shows the average absorbance spectrum of lysozyme, using transmission spectra from Figure 17.

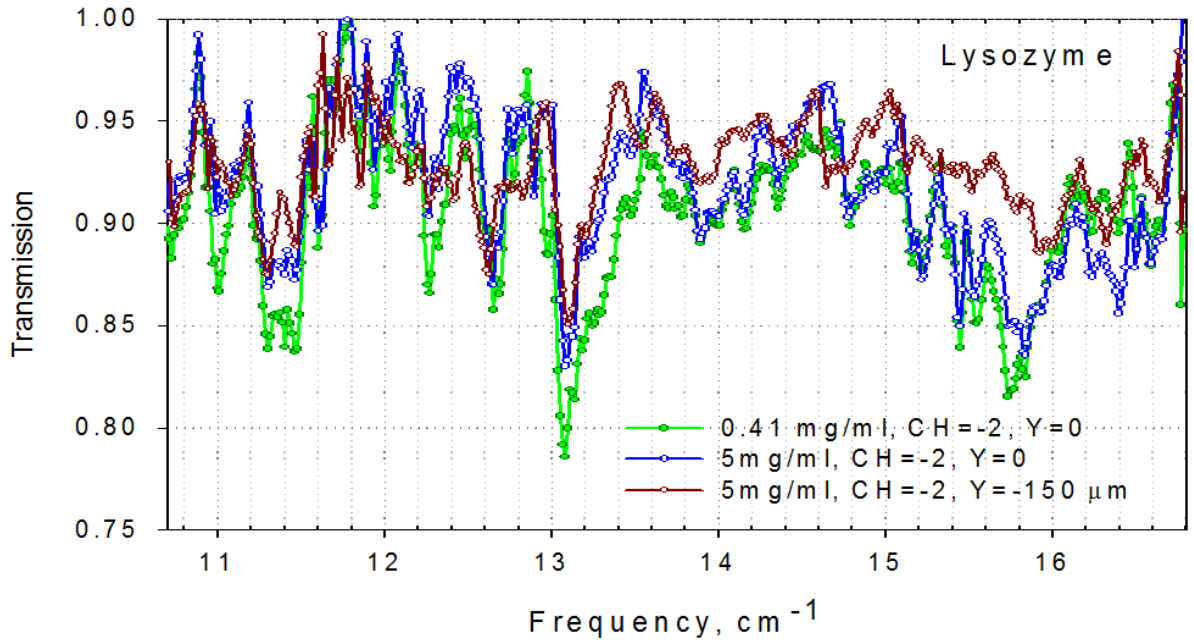

Figure 17. Transmission spectra of lysozyme at two different concentrations (0.41 and 5 mg/mL, which are shown as green and blue lines, respectively) and at two different y-axis locations on the microchannels sample chip (y = 0 and –150 μm, which are shown as blue and brown lines, respectively).

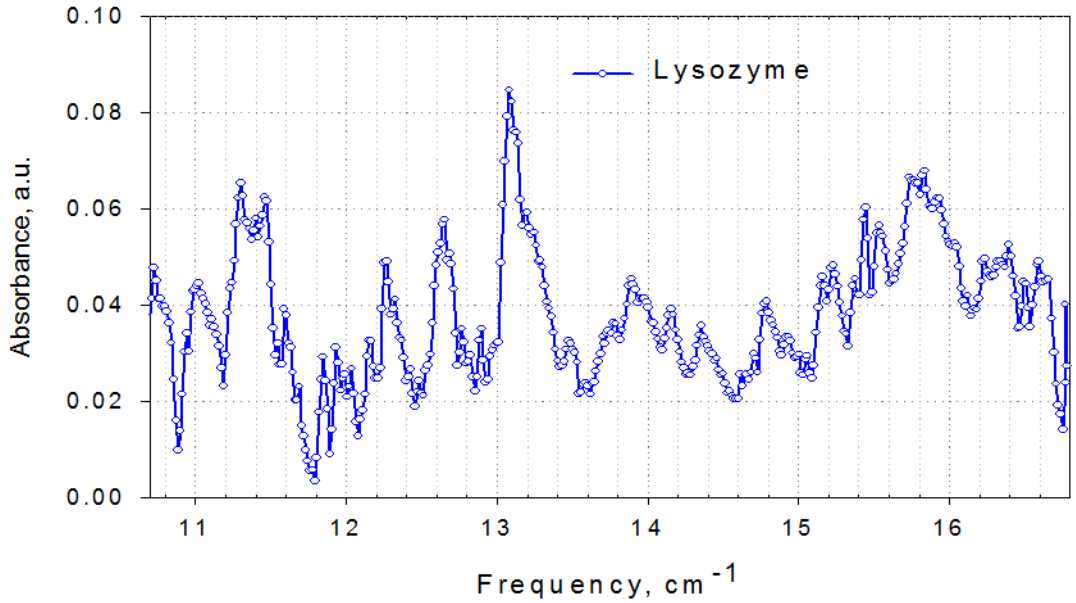

Figure 18. Averaged absorbance spectrum of lysozyme using transmission spectra from Figure 17.

4.2.2 Lysozyme THz MD Simulation

Because the lysozyme molecule was much larger in size, as compared with insulin, it was expected to produce many more spectral peaks than would insulin, and these spectral peaks could overlap.

There were several 3D molecular structures for lysozyme available in the PDB file. These included: (1) 1BWH, (2) 1LYS, and (3) 4QEQ PDB structures, which were determined by X-ray analysis. It was important to choose the structure that most closely correlated with that of the purchased and analyzed lysozyme material. The structure 1BWH had already been obtained with a low-resolution X-ray system. The 4QEQ PDB structure was obtained with a higher-resolution X-ray system. The X-ray crystal structures of 4QEQ and 1LYS can be found at the PDB website (*17, 18*). According to these global validation metrics criteria, the 4QEQ structure had better Ramachandran (*19*) and sidechain outlier scores than did 1BWH or 1LYS, which meant that the 4QEQ structure was of better quality.

Several MD simulations were conducted using the 1BWH PDB structure with three different initial random atomic velocities and with E_{TOT} at room temperature (293 K) and at an elevated temperature of 298 K.

For example, Figures 19 and 20 show progress in the simulation predictive capability for lysozyme. Figure 19 shows the lysozyme MD simulation results at room temperature, T = 293 K. Three different plots, calculated at three different total energies of a protein (E_{TOT} = –50947, –50915, and –50888 kcal/mol, which are shown as blue, pink, and green lines, respectively, in Figure 19), show that these spectra were sensitive to the E_{TOT} values used

even though experiments were carried out at room temperature. This could be expected because the lysozyme melting temperature under pH 7 is only 71 °C (*25*), and it is not far enough from room temperature. This means that a change in the measurement temperature can strongly affect the spectrum. For this reason, we also conducted a simulation not only at T = 293 K, but also at T = 298 K, which was the temperature near the spectrometer at the time of measurement. Figure 20 shows the lysozyme absorption spectrum that was simulated for 298 K.

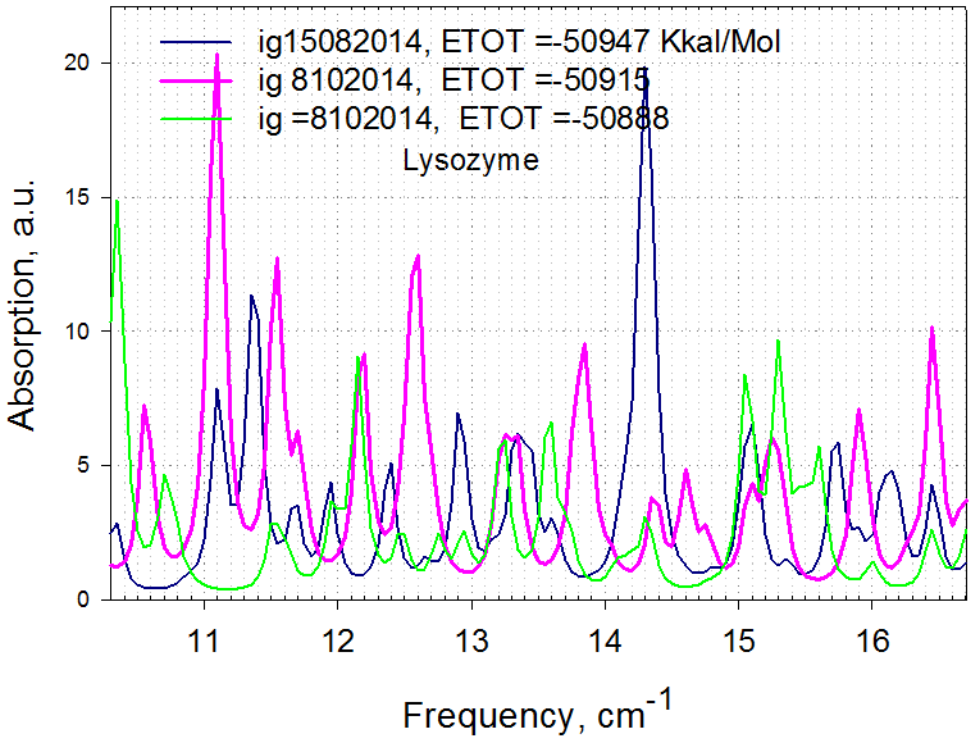

Figure 19. Lysozyme MD simulation results at room temperature, T = 293 K. Three different plots, calculated at three different total energies of a protein (E_{TOT} = –50947, –50915, and –50888 kcal/mol, which are shown as blue, pink, and green lines, respectively).

Four different MD simulations were performed at different E_{TOT} values, as shown in Figures 19 and 20. The MD simulation at E_{TOT} = –52260 kcal/mol shows a better correlation with the experimental measurement (Figure 20) than with the other three spectra (Figure 19). Although the correlation between MD simulation at E_{TOT} = –52260 kcal/mol and the experimental measurement, as shown in Figure 20, showed that some measured absorption peaks occurred at the same frequency as in simulation, the results were not favorable. The next MD simulation was made using different E_{TOT} values to increase correlation results and to get close to a 100% match with all experimental peaks.

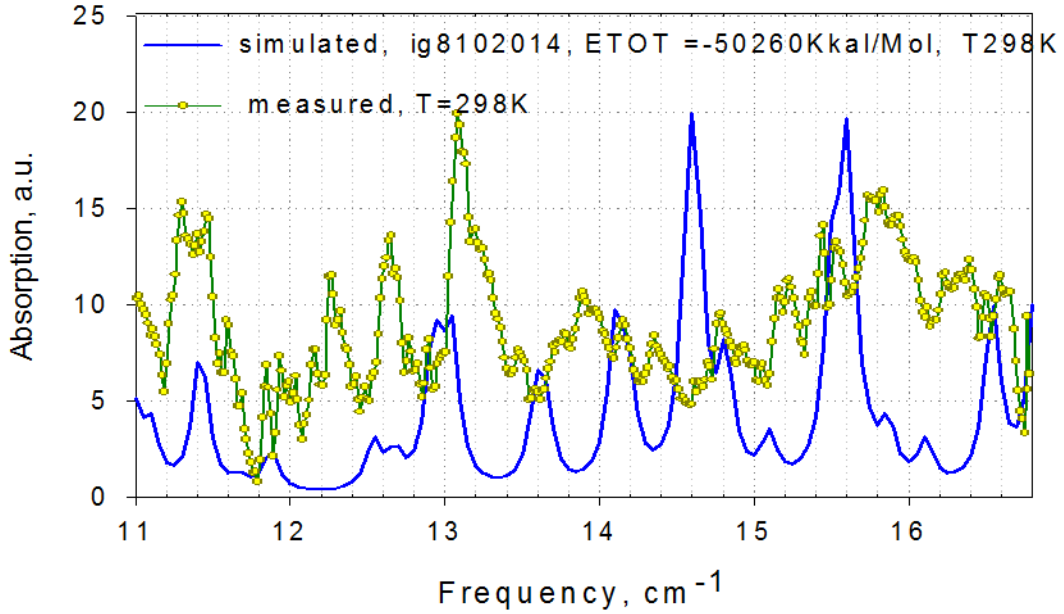

Figure 20. Lysozyme THz MD simulation absorption spectrum, which was simulated with the PDB file 1BWH using a room temperature value of T = 298 K and at the single total energy of a protein, E_{TOT} = –50260 kcal/mol.

In addition, as was the case with insulin, it was necessary to explore more than one crystal structure from those available in the PDB. MD simulation modeling was conducted with two more crystal structures using two new PDB files: (1) 1LYS and (2) 4QEQ, which provide slightly different atomic positions. Figure 21 compares the two THz MD simulations that used the two PDB files (4QEQ and 1LYS, which are shown as brown and pink lines, respectively) at T = 298 K (without Cl^- ions) with experimental THz spectra (green lines).

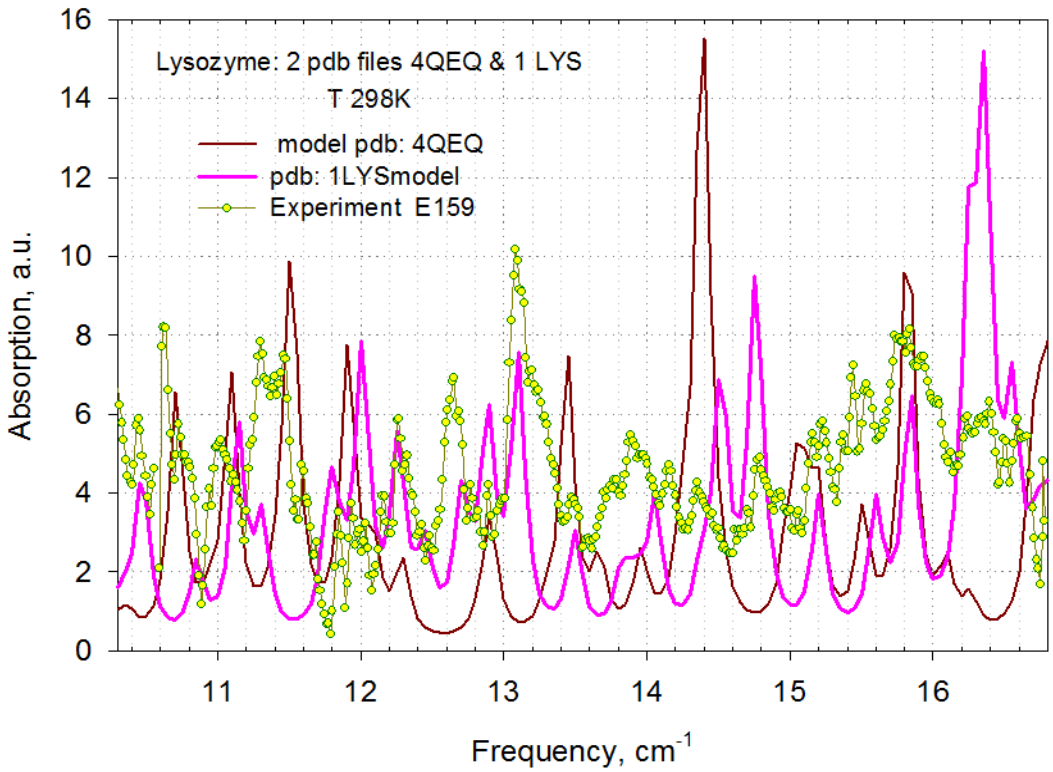

Figure 21. Two THz MD simulations using two PDB files (4QEQ and 1LYS, which are shown as brown and pink lines, respectively) at T = 298 K (without Cl^- ions) with experimental THz spectra (green line).

Although many peaks in the simulated and experimental data have the same or very similar frequencies, MD simulations were also conducted with two lysozyme structures and Cl^- ions added to the model (system of protein and water) because these ions were present in the experimental material. The results are shown in Figures 22 and 23. Figure 22 shows the THz absorption spectra from an MD simulation using two model structures (4QEQ and 1LYS, which are shown as brown and pink lines, respectively) with Cl^- ions.

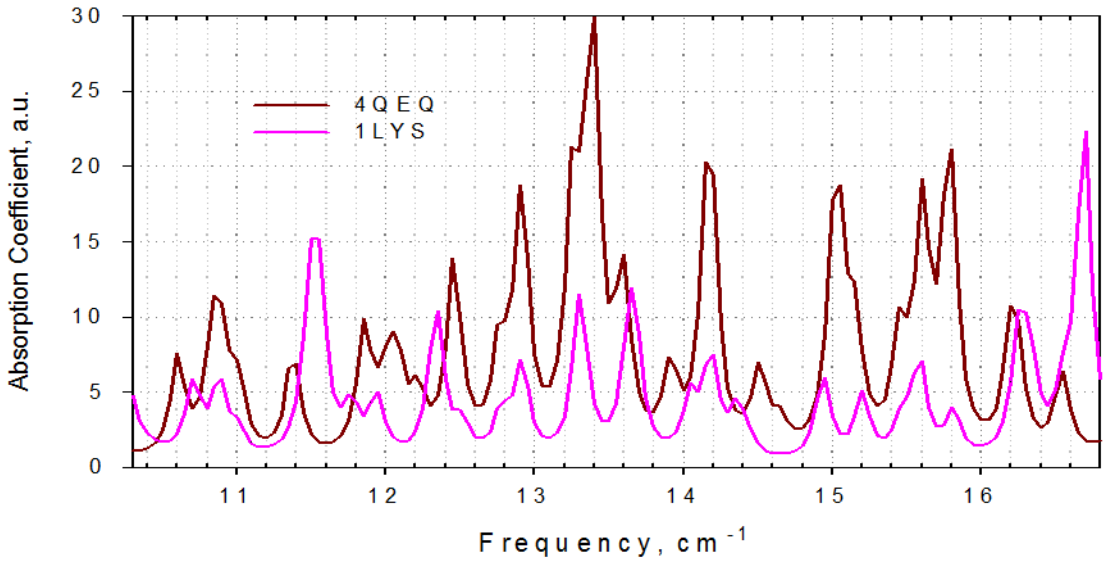

Figure 22. THz absorption spectra from an MD simulation using two model structures (4QEQ and 1LYS, which are shown as brown and pink lines, respectively) with Cl^- ions.

Figure 23 shows a comparison between two THz absorption spectra, one from an MD simulation using PDB file 4QEQ with Cl^- ions (brown line) and the other from experimental THz measurements (T = 298 K) (green line). In Figure 23, the lysozyme MD simulation spectra used an averaging correlation matrix interval of 100 ps.

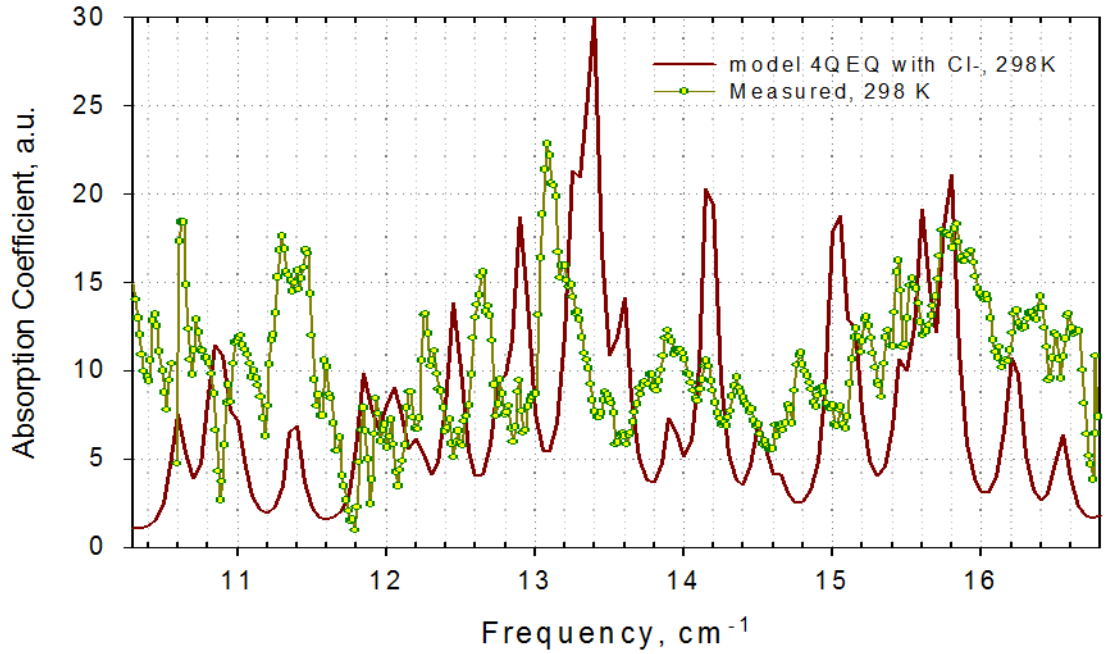

Figure 23. Comparison between two THz absorption spectra from an MD simulation using PDB file 4QEQ with Cl^- ions (dark red line) and from experimental THz measurements at T = 298 K (green line).

As expected and shown Figure 23, the THz absorption spectrum using PDB file 4QEQ with Cl^- ions (brown line) shows a closer correlation with the experimentally measured THz spectrum (green line). THz MD simulated spectra were, however, dependent on several parameters that were not yet optimized. Additional efforts sought to improve the convergence between MD simulation and experimental spectra by using optimizing simulation parameters, as shown in Figure 24.

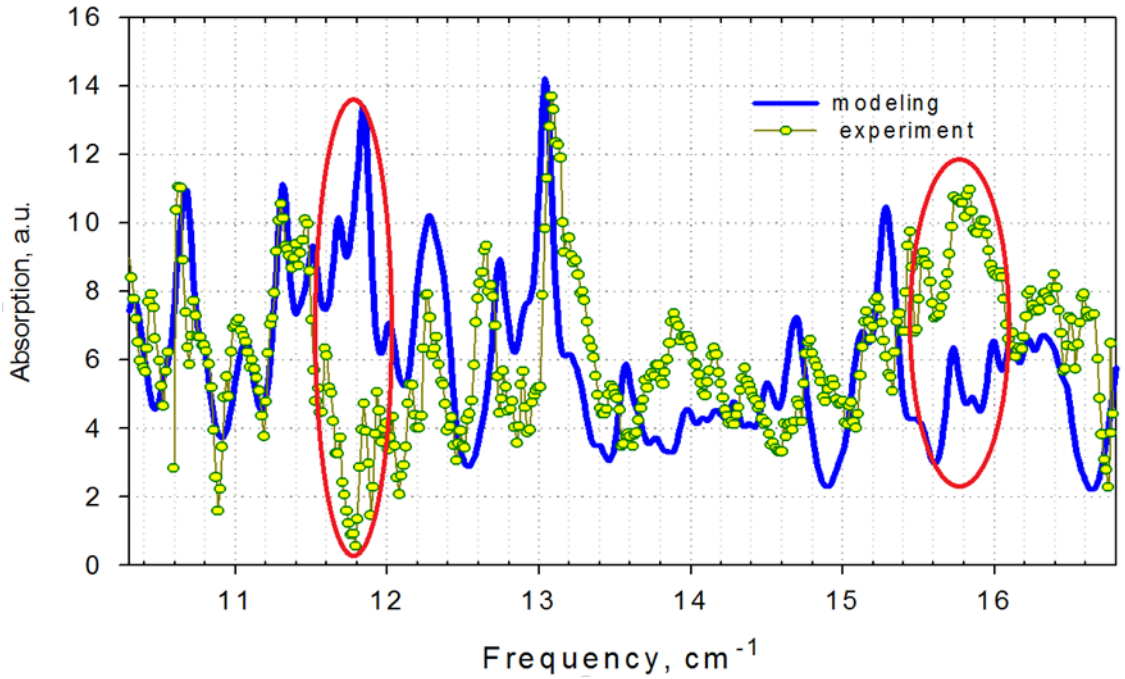

Figure 24. Lysozyme experimental THz spectrum (green plot) and THz MD spectrum (blue line) determined using averaging correlation matrices for five intervals: 20, 30, 40, 50, and 60 ps.

Figure 24 shows the lysozyme experimental THz spectrum (green line) and THz MD spectrum (blue line) that were determined using averaging correlation matrices for five intervals: 20, 30, 40, 50, and 60 ps, and not just one time interval (100 ps), as is shown in Figure 23 (brown line). Figure 24 shows better correlation between the experimental and MD simulation spectra of lysozyme. The two red oval regions indicate the main discrepancies observed in this evaluation. Simulated lysozyme spectra are sensitive to the initial atomic position provided by PDB files. It was important to explore several PDB crystal structures and conduct simulations with Cl^- ions to determine whether the interaction with ions was responsible for some features in experimental spectra and to resolve the discrepancies. It was found that the correlation between the experimental data and MD simulation resulted in peak position differences on a frequency scale of <0.1 cm^{-1} and with good relative peak intensities.

We evaluated the dominant THz peak at about 13 cm^{-1}, shown in Figure 24, to understand the primary causes of vibrations, as detailed in Figure 25. Figure 25a shows the same graph as Figure 24, with two highlighted regions of discrepancies (red ovals) between the MD

simulation and the experimental spectrum. In Figure 25b, a quasi-harmonic analysis of the 13 cm^{-1} resonant frequency reveals that arginine 128 and glutamine 121 residues have the highest oscillation amplitudes in the *z* direction as compared with the other residues. The atoms that make the biggest contribution to the oscillations are marked by spheres (white for hydrogen, blue for nitrogen, red for oxygen, and grey for carbon). Figure 25c shows the variation over time in the distance between glutamine 121 and arginine 128 residues in the *z* direction. The amplitude was extremely large at ~1 Å.

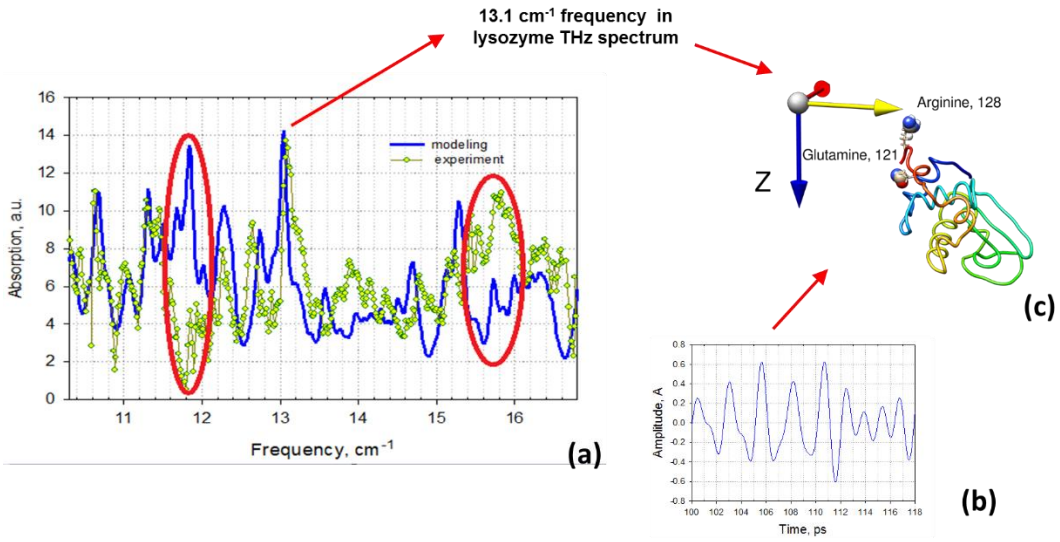

Figure 25. Diagram of a potential method to speed up MD simulations: (a) same graphic as that of Figure 24, with attention on the dominant vibrational peak at about 13 cm^{-1}; (b) quasi-harmonic analysis of the 13 cm^{-1} resonant frequency reveals that arginine 128 and glutamine 121 residues have highest oscillation; and (c) variation over time of the distance between glutamine 121 and arginine 128 residues in the *z* direction.

MD simulation using multiple time intervals, as shown in Figure 24, improved its correlation with the experimental THz spectra of lysozyme. It also provided an in-depth understanding of the responsible vibrations. Unfortunately, each MD simulation takes a few days to generate. Figure 25 shows a new approach that can be used to speed up the MD simulation. Using this method, individual experimental THz spectroscopic THz vibrational peaks are interrogated and modeled, but the entire frequency range is not. In Figure 25, evaluation of the 13 cm^{-1} resonant frequency revealed that arginine 128 and glutamine 121 residues had the highest oscillation amplitudes in the *z* direction as compared with the other residues. Arginine 128 and glutamine 121 were the primary causes of the 13 cm^{-1} peak, regardless of the chosen PDB file structure (4QEQ or 1LYS). Fine tuning the 13 cm^{-1} peak was accomplished much more rapidly by using MD simulation for only the arginine 128 and glutamine 121 with different settings, rather than by using the previous MD simulation approach in which all atoms and entities in the structure were analyzed. This new approach will significantly reduce the MD simulation time and improve our understanding of the underlying mechanisms that produce experimental THz peaks.

4.3 Bacteria THz Study

4.3.1 Bacteria THz Experimental Spectra

A microsyringe was used to deposit the *B. subtilis* var. *niger* spore suspension in the correct location and amount. Unfortunately, when the 0.05 µL droplet of bacteria in suspension dried, it formed a "coffee ring" as shown in Figure 26. Most of the bacteria suspended in the droplet moved to the edge, which left a ring of bacteria after drying. Therefore, the THz detector tip had to be moved to the edge of the dried droplet for this study, which required the use of a second vertical camera to provide a top view for precise ring-edge location.

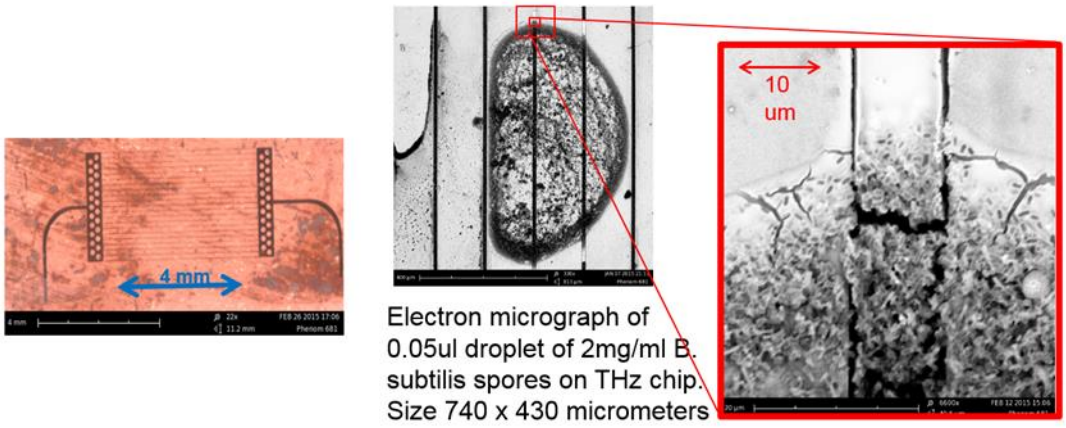

Figure 26. Drying behavior for a 0.05 µL droplet of 2 mg/mL of *B. subtilis* spores on a THz microchannel sample chip holder (evaporated to leave a ring similar to a "coffee-ring" effect).

The *E. coli* cell studies presented in the next several paragraphs are found in an article by Globus et al. and are used to show the capability of the VsTHz system with bacterial cells (*9*).

To demonstrate the capabilities of the VsTHz spectrometer, transmission spectra from bacterial cells and some of their molecular components (DNA and thioredoxin) were measured and recalculated for the absorption coefficient per mass of material as described by Globus et al. (*2*). The reliability of the transmission results was verified by measuring samples with different amounts of material and at different coordinates in the microchannel array. Figure 27 shows the transmission spectra of *E. coli* cells in two different amounts, 1 and 2 µL. The two spectra show good correlation (reproducibility) between the frequency locations of the spectral features and the transmission. In addition, the absorption was generally higher (lower transmission values) for the 2 µL sample, which indicated that the absorption was from the sample.

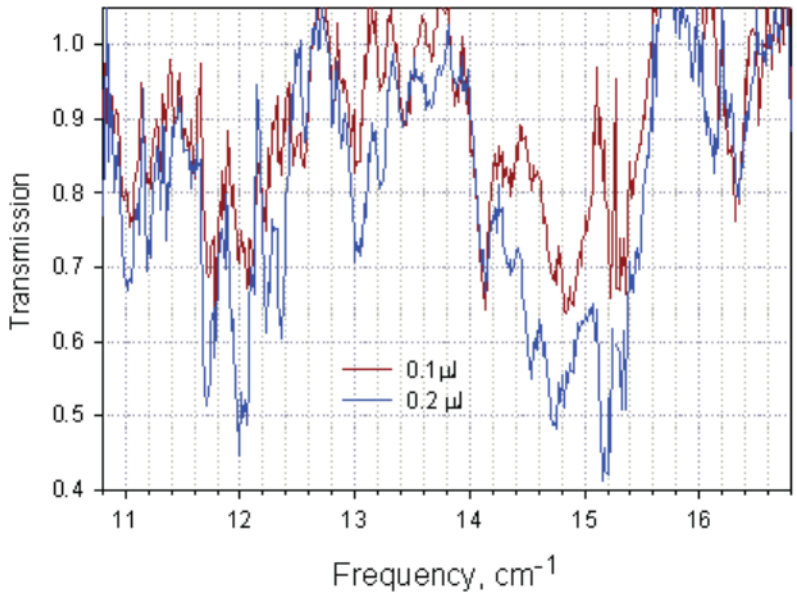

Figure 27. Transmission of *E. coli* cells using two samples with different amounts of material.

Figure 28 shows the absorbance spectra from one droplet (blue line) and two droplets (brown line) of *B. subtilis* spores. Each droplet size was 0.05 µL, contained 0.2 µg of *B. subtilis* material, and spread in an area of 0.3 mm in diameter. The *B. subtilis* sample concentration was 4 mg/mL.

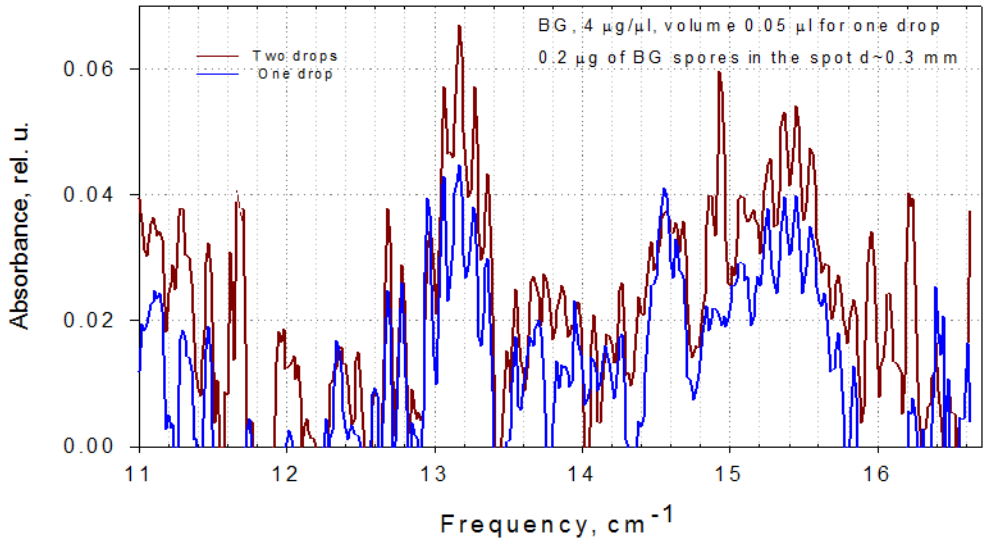

Figure 28. Absorbance spectra of *B. subtilis* spores from 0.05 µL (blue line, 1 droplet) and 0.1 µL (brown line, 2 droplets). *B. subtilis* spore sample concentration was 4 mg/mL.

Transmission and absorption spectra of *E. coli* DNA are shown in Figures 29 and 30. Very narrow spectral lines were detected, with widths of ~0.1–0.2 cm^{-1}. The peak positions were preserved in the spectra of samples having different amounts of material, but the intensities of the absorption peaks calculated per unit mass were often reduced for larger sample amounts (Figure 30).

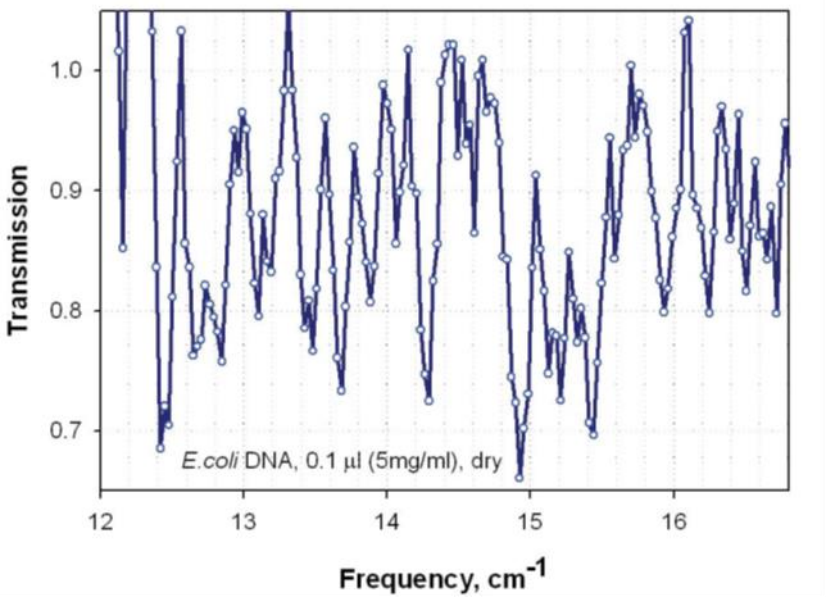

Figure 29. Transmission spectrum of *E. coli* DNA with 500 ng of material in the droplet.

We assumed that the thickness of the sample material after drying (at the edge of the ring) was proportional to its mass, which was determined from the volume of solution and the concentration of material in solution. This gave us the mass of solid material in the drop after evaporation of water. We further assumed that the spot area was the same when more material was added. However, at the time of this study, we could not control the spot size and could not be sure that this area was the same. This may explain the apparent dependence of absorption coefficient on mass, as shown in Figure 30.

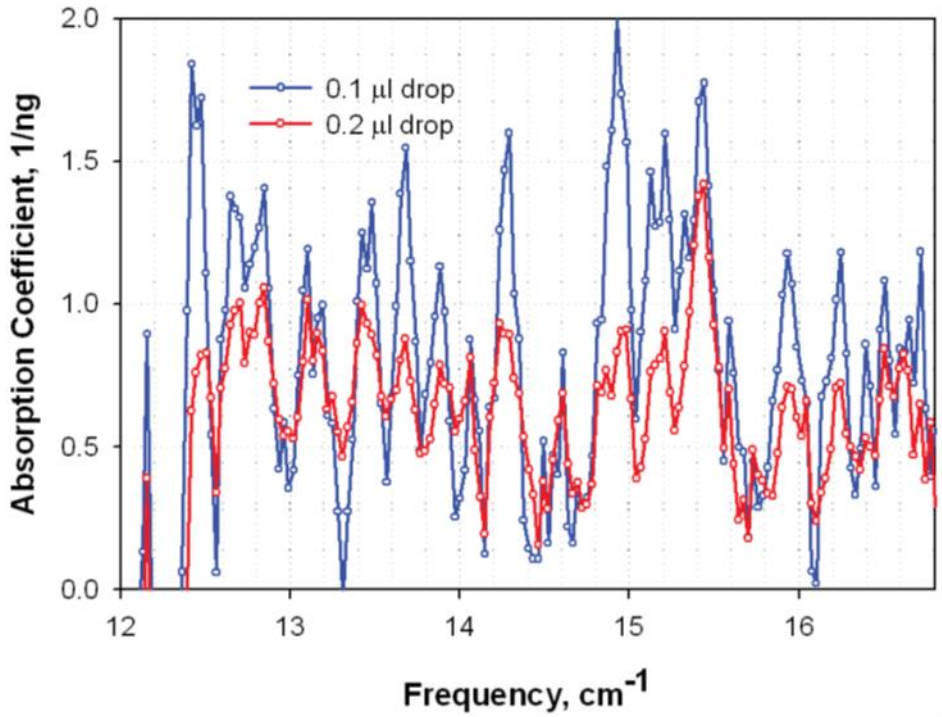

Figure 30. Absorption coefficient spectra of *E. coli* DNA. Scaling was not observed with the amount of sample material studied.

As shown in this and in earlier work by Globus et al. (*2*), spectral lines are sharper in thin samples, and they have significant broadening and damping of spectral features in bulk samples that is probably because of less-oriented material. Very thick samples usually do not provide well-resolved spectral features in the sub-THz region. This effect can explain the sensitivity of sub-THz spectroscopic characterization to the specific sample preparation techniques.

Further development of the sample delivery approach is expected to provide increased reproducibility and efficiency because the sample presentation in the spectrometer detection region will be more accurate and controlled.

Figure 31 compares the averaged transmission spectra of *E. coli* cells, as measured on the Bruker FTIR spectrometer (IFS 66v), with the results from the VsTHz spectrometer. Different transmission scales were used for the two instruments, and a significantly reduced amount of sample was used. Overlapping spectral peaks (narrow and intense spectral lines) in the spectrum, measured by the Bruker FTIR instrument, are resolved by the VsTHz spectrometer.

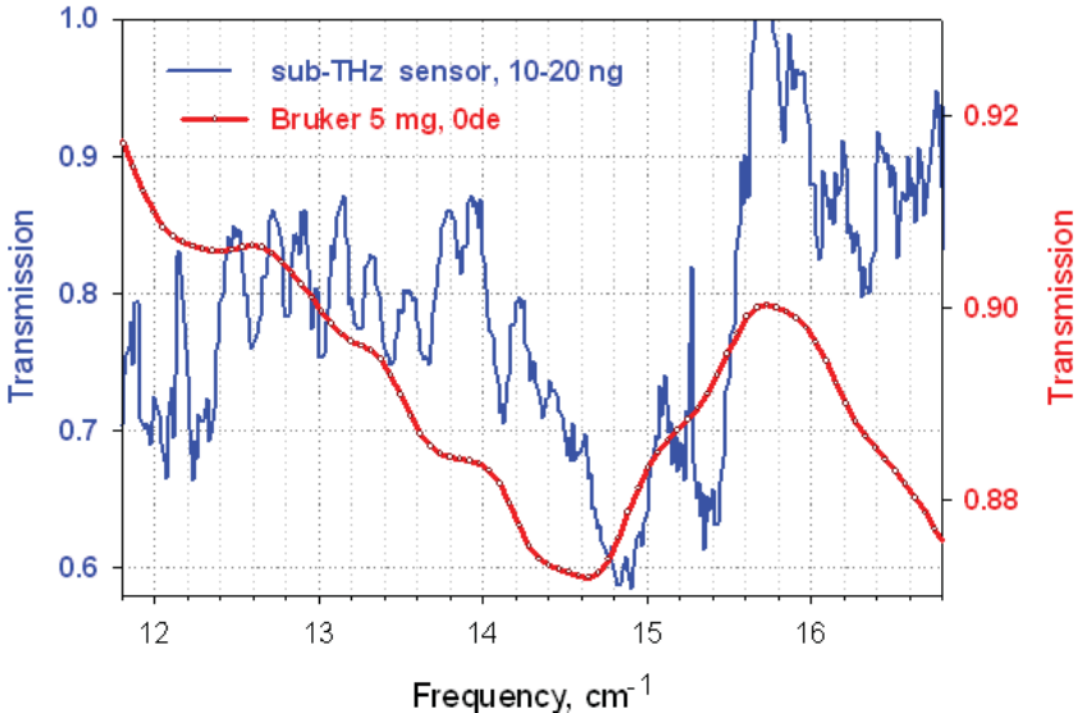

Figure 31. Transmission spectra of *E. coli* cells measured with two different instruments, the Bruker FTIR (IFS 66v, red line) and the VsTHz frequency-domain spectroscopic sensor (blue line).

There was a shift in the major transmission minimum position from 14.6 to 14.9 cm^{-1}. This 0.3 cm^{-1} shift to a higher frequency was explained by the different orientations of the cells in the two setups, which were needed because spectra are sensitive to the orientation of biomaterial with respect to the electric field vector in THz radiation (*2*).

Comparison of the parameters and conditions used with the new VsTHz spectrometer with those of the Bruker spectrometer IFS 66v in the sub-THz operational range (11–17 cm^{-1}) has demonstrated an order of magnitude better spectral resolution and 10–15 times higher peak intensities.

The high sensitivity of the VsTHz spectrometer allowed 2 orders of magnitude less sample to be deposited on the sample chip (yielding a spot of 1–2 mm^2). The VsTHz detector waveguide interrogates and acquires signals on only a fraction of a 1–2 mm^2 sample spot because the detector antenna is only 0.12 × 0.15 mm in size.

Because overlapping of individual resonances was still possible, the estimates for the dissipation factor from the width of spectral lines in Figures 28–30 provided an upper limit for γ between 0.1 and 0.2 cm^{-1}.

4.3.2 Bacteria THz MD Simulation

Unfortunately, because any bacterial cell consists of many biomolecules and chemicals, and because PDB files do not exist for bacteria, an MD simulation could not be performed. But part of a cell's biography can be modeled as described in this section.

Figure 32 shows the experimental spectra of the *E. coli* protein thioredoxin, with computational modeling results using MD simulations and a damping factor of $\gamma = 0.12$ cm^{-1}. These results were used to confirm the existence of the observed narrow and intense resonance features in the sub-THz transmission and the absorption spectra of biological materials, as measured with VsTHz spectrometer.

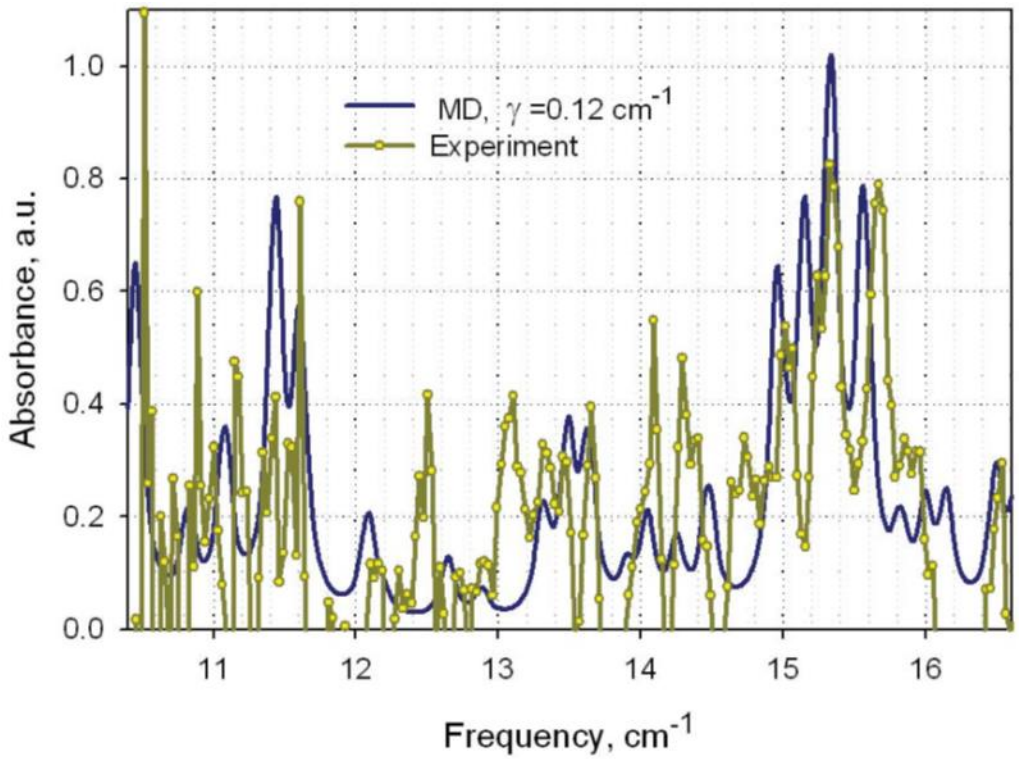

Figure 32. Absorption spectra of protein thioredoxin from *E. coli*, obtained using MD simulation and experimental results from the VsTHz spectrometer.

The computational modeling procedure was conducted exactly as it was described in detail by Alijabbari et al. (*3*). The only difference was that a smaller value of the dissipation factor (0.12 cm^{-1}) was used in this study, which was close to the approximate experimental widths of spectral features observed with the VsTHz spectrometer. Not all peaks (as shown in Figure 32) were reproduced in the measured and simulated spectra. Simulation parameters have not yet been optimized, and the same value of γ was used to calculate absorption for all vibrational modes.

Initial MD simulation and experimental THz spectra confirmed the existence of intense and narrow absorption lines, which can be used for discrimination between different bacteria and strains. The narrow absorption lines were confirmed in an article by Qiu et al. (*6*) from τ scales in thioredoxin from femtosecond-resolved fluorescence spectroscopy experiments. The aforementioned authors (*6*) also observed longer quenching dynamic processes with time scales of 275–615 ps at a hydrogen bond distance, which can give local fluctuations with vibration spectral line widths of <0.1 cm^{-1}.

5. CONCLUSIONS

The VsTHz spectrometer (frequency-domain THz spectroscopic system prototype, operating at room temperature) was tested with a variety of biological samples. This prototype system provided high spectral resolution and significantly improved detection sensitivity and reliability in the sub-THz operational range as compared with commercially available spectrometers. The results of this study demonstrated highly resolved transmission (absorption) spectra from only 10–20 ng of biological macromolecules, bacterial cells, and spores.

The experimental results revealed very intense and narrow spectral features from biological molecules and bacteria with widths of ~0.1–0.2 cm^{-1}. The results provided completely new information about the interactions between THz radiation and biological materials, which confirmed the diverse relaxation dynamic mechanisms that are relevant to sub-THz spectroscopy. This demonstration of multiple intense and specific resonance features provides potential conditions for the reliable discriminative capabilities of this technology to the level of bacterial strains in extremely small sample volumes. However, further evaluation is required to fully assess the limits of these capabilities.

Experimental results and improvements on the existing VsTHz spectrometer will create a foundation for the development of new types of advanced biological THz systems. In addition, this new instrument can be used for monitoring interactions between biomaterials and reagents and for studying conformational changes and biomedical processes in near real time.

Improvements that are important for improved computational modeling include the following: finding the PDB structures that best represent the experimental material; more accurately representing components of the protein surroundings such as water, ion molecules, and so on; and averaging the results from several runs while varying the equilibration parameters. Finally, using quasi-harmonic analysis of individual resonant frequencies, and using that information to optimize the MD simulation can result in greatly improved simulation times.

Future experimental efforts should include further investigation regarding the role of sample thickness, location, water content, and freshness (changing the absorption spectrum of the sample material due to degradation). In addition, future efforts should also strive to increase the number of experimental runs on each sample to ensure a good statistical representation of the in-class diversity. Finally, statistical methods such as “Principal Component Analysis” should be used to quantify the correlations between the MD-simulated and experimental THz spectra.

Blank

LITERATURE CITED

1. Heilweil, E.J.; Plusquelic, D.F. Terahertz Spectroscopy of Biomolecules. In *Terahertz Spectroscopy*; Taylor and Francis: London, 2008; Chapter 7, pp 269–297.

2. Globus, T.; Dorofeeva, T.; Sizov, I.; Gelmont, B.; Lvovska, M.; Khromova, T.; Chertihin, O.; Koryakina, Y. Sub-THz Vibrational Spectroscopy of Bacterial Cells and Molecular Components. *Am. J. Biomed. Eng*. **2012,** *2* (4), 143–154.

3. Alijabbari, N.; Chen, Y.; Sizov, I.; Globus, T.; Gelmont, B. Molecular Dynamics Modeling of the Sub-THz Vibrational Absorption of Thioredoxin from *E. coli*. *J. Mol. Model*, **2012,** *18* (5), 2209–2218.

4. Li, T.; Hassanali, A.A.; Kao, Y.T.; Zhong, D.; Singer, S.J. Hydration Dynamics and Time Scales of Coupled Water-Protein Fluctuations. *J. Am. Chem. Soc.* **2007,** *129* (11), 3376–3382.

5. Furse, K.E.; Corcelli, S.A. Molecular Dynamics Simulations of DNA Solvation Dynamics. *J. Phys. Chem. Lett.* **2010,** *1* (12), 1813–1820.

6. Qiu, W.; Wang, L.; Lu, W.; Boechler, A.; Sanders, D.A.R.; Zhong, D. Dissection of Complex Protein Dynamics in Human Thioredoxin. *PNAS* **2007,** *104* (13), 5366–5371.

7. Globus, T.; Moyer, A.; Gelmont, B.; Sizov, I.; Khromova, T. Dissipation Time in Molecular Dynamics and Discriminative Capability for Sub-Terahertz Spectroscopic Characterization of Bio-Simulants. In *Proceedings of the 2011 Defense Threat Reduction Agency Chemical and Biological Defense Science and Technology Conference*, Las Vegas, NV, 2011.

8. Woolard, D. *Spectroscopic Imaging Technology for THz Biosensor Integrated with a Lab-On-Chip Platform*; Technical Report CBD10-110-0099; U.S. Army Research Office: Research Triangle Park, NC, May 2010.

9. Globus, T.; Moyer, A.; Gelmont, B.; Khromova, T.; Lvovska, M.; Sizov, I.; Ferrance, J. Highly Resolved Sub-THz Vibrational Spectroscopy of Biological Macromolecules and Cells. *IEEE Sensors J*. **2012,** *13* (1), 72–79.

10. Globus, T; Moyer, A.; Gelmont, B.; Khromova, T.; Sizov, I.; Ferrance, J. Sub-Terahertz Resonance Spectroscopy of Biological Macromolecules and Cells. In *Proceedings of SPIE—The International Society for Optical Engineering*, Vol. 8716N; Conference on Terahertz Physics, Devices, and Systems VII: Advanced Applications in Industry and Defense, Baltimore, MD, 29–30 April 2013; SPIE: Bellingham, WA, 2013.

11. Parthasarathy, R.; Bykhovski, A.; Gelmont, B.; Globus, T.; Swami, N.; Woolard, D.L. Enhanced Coupling of Subterahertz Radiation with Semiconductor Periodic Slot Arrays. *Phys. Rev. Lett.* **2007,** *98* (15), 153906-1–153906-4.

12. Gelmont, B.; Parthasarathy, R.; Globus, T.; Bykhovski, A.; Swami, N. Terahertz (THz) Electromagnetic Field Enhancement in Periodic Subwavelength Structures. *IEEE Sens. J.* **2008,** *8* (5–6), 791–796.

13. Gelmont, B.; Globus, T. Edge Effect in Perfectly Conducting Periodic Subwavelength Structures. *IEEE Trans. Nanotechnol*. **2011,** *10* (1), 83–87.

14. Gelmont, B.; Globus, T.; Bykhovski, A.; Lichtenberger, A.; Swami, N.; Parthasarathy, R.; Weikle, R. Method of Local Electro-Magnetic Field Enhancement of Terahertz (THz) Radiation in Sub-Wavelength Regions and Improved Coupling of Radiation to Materials through the Use of the Discontinuity Edge Effect. U.S. Patent WO2,008,109,706 A1, 5 March 2008.

15. Bass, R.; Lichtenberger, A.; Weikle, R.; Pan, S.; Bryerton, E.; Walker, C. Ultrathin Silicon Chips for Submillimeter Wave Applications. In *Proceedings of the 15th International Symposium on Space Terahertz Technology*, 27–29 April 2004; Northampton, MA, pp 392–399.

16. Blundell, T.L.; Cutfield, J.F.; Cutfield, S.M.; Dodson, E.J.; Dodson, G.G.; Hodgkin, D.C.; Mercola, D.A.; Vijayan, M. Atomic Positions in Rhombohedral 2-Zinc Insulin Crystals. *Nature* **1971,** *231* (5304), 506–511.

17. Worldwide Protein Data Bank http://ftp.wwPDB.org/pub/PDB/validation_reports/qe/4qeq/4qeq_full_validation. PDB file for 4QEQ (accessed January 2015 and January 2016).

18. Worldwide Protein Data Bank http://ftp.wwPDB.org/pub/PDB/validation_reports/ly/1LYS/1LYS_full_validation. PDB file for 1LYS (accessed January 2015 and January 2016).

19. Ramachandran Plot. http://en.wikipedia.org/wiki/Ramachandran plot (accessed January 2015 and January 2016).

20. Karplus, M.; Kushick, J.N. Method for Estimating the Configurational Entropy of Macromolecules. *Macromolecules* **1981,** *14* (2), 325–332.

21. Levy, R.M.; Karplus, M.; Kushick, J.; Perahia, D. Evaluation of the Configurational Entropy for Proteins: Application to Molecular Dynamics Simulations of an α-Helix. *Macromolecules* **1984,** *17* (7), 1370–1374.

22. Globus, T.; Woolard, D.L.; Bykhovskaia, M.; Gelmont, B.; Werbos, L.; Samuels, A. THz-Frequency Spectroscopic Sensing of DNA and Related Biological Materials. *Int. J. High Speed Electro. Syst.* **2003,** *13* (4), 903–936.

23. Sambrook, J.; Fritsch, E.F.; Maniatis, T. *Molecular Cloning: A Laboratory Manual*, 2nd ed.; Cold Spring Harbor Laboratory Press: Cold Spring Harbor, NY, 1989; Vol. 3.

24. Haas, M.J.; Dowding, J.E. Aminoglycoside-Modifying Enzymes. *Methods Enzymol*. **1975,** *43*, 611–628.

25. Blumlein, A.; McManus, J.J. Reversible and Non-Reversible Thermal Denaturation of Lysozyme with Varying pH at Low Ionic Strength. *Biochim. Biophys. Acta* **2013,** *1834* (10), 2064–2070.

Blank

ACRONYMS AND ABBREVIATIONS

3D	three-dimensional
$\alpha(\nu)$	absorption coefficient spectra
γ	damping factor
τ	molecular dynamics relaxation time
ν	frequency
ν_k	normal mode frequencies
A	absorbance
AMBER	assisted model building with energy refinement (simulation program)
E_{TOT}	total energy of a molecular system
F	force constant
FFT	fast Fourier transform
FTIR	Fourier transform infrared (spectrometry)
k	vibrational modes
MD	molecular dynamic
NPT	constant number, pressure, and temperature ensemble
NVE	constant number, volume, and energy ensemble
NVT	constant number, volume, and temperature ensemble
PDB	protein data bank
R_iR_k	random displacement value between atom i and atom k
S_k	oscillator strength
sub-THz	sub-terahertz
T	temperature
$\check{T}$	transmission
THz	terahertz
VDI	Virginia Diodes, Inc.
VsTHz	Vibratess sub-terahertz (system)
W	spectral line width

DISTRIBUTION LIST

The following individuals and organizations were provided with one Adobe portable document format (pdf) electronic version of this report:

U.S. Army Edgewood Chemical
Biological Center (ECBC)
Spectroscopy Branch
RDCB-DRI-S
ATTN: Maswadeh, W.
Vanderbeek, R.
Moon, R.
Tripathi, A.

Defense Threat Reduction Agency
DTRA/RD-CBD T
ATTN: Ward, T.
J9-CBS
ATTN: Moore, E.

Department of Homeland Security
DHS ORD CSAC
ATTN: Famini, G.

G-3 History Office
U.S. Army RDECOM
ATTN: Smart, J.

ECBC Technical Library
RDCB-DRB-BL
ATTN: Foppiano, S.
Stein, J.

Office of the Chief Counsel
AMSRD-CC
ATTN: Upchurch, V.

Defense Technical Information Center
ATTN: DTIC OA

ECBC Rock Island
RDCB-DES
ATTN: Lee, K.


EDGEWOOD CHEMICAL BIOLOGICAL CENTER
A U.S. Army RDECOM Laboratory